Fenton, C. R., Niedermann, S., Goethals, M. M., Schneider, B., Wijbrans, J. (2009): Evaluation of cosmogenic He-3 and Ne-21 production rates in olivine and pyroxene from two Pleistocene basalt flows, western Grand Canyon, AZ, USA. - Quaternary Geochronology, 4, 6, 475-492

DOI: 10.1016/j.quageo.2009.08.002

Evaluation of cosmogenic ^{3}He and ^{21}Ne production rates in olivine and pyroxene from two Pleistocene basalt flows, western Grand Canyon, AZ, USA

Cassandra R. Fenton[*, 1, 2]

Samuel Niedermann[1]

Mirjam M. Goethals [1,3]

Björn Schneider[4]

Jan Wijbrans[4]

[*]Corresponding author: Email: C.Fenton@suerc.gla.ac.uk

[1] Helmholtz-Zentrum Potsdam – Deutsches GeoForschungsZentrum, Telegrafenberg, D-14473 Potsdam, Germany; nied@gfz-potsdam.de

[2] Current contact information: NERC Cosmogenic Isotope Facility (CIAF) at Scottish Universities Environmental Research Centre, Scottish Enterprise Technology Park, East Kilbride G75 0QF, United Kingdom; Phone: +44 (0)1355 270161 Fax: +44(0)1355 229898

[3] Geologisch-Paläontologisches Institut, Westfälische Wilhelms-Universität Münster, Corrensstr. 24, D-48149 Münster, Germany; mirjamgoethals@yahoo.com

[4] Vrije Universiteit Amsterdam, Department of Isotope Geochemistry, De Boelelaan 1085, 1081 HV Amsterdam, The Netherlands; bjoern.schneider@falw.vu.nl, jan.wijbrans@falw.vu.nl

Submitted for publication in Quaternary Geochronology

Revised version, July 16, 2009

keywords: cosmogenic, helium, neon, olivine, pyroxene, basalt, production rates

Abstract

Combining cosmogenic ^{3}He and ^{21}Ne ($^{3}He_c$ and $^{21}Ne_c$) measurements on both pyroxene and olivine from the Pleistocene Bar Ten flows (85 -107 ka) greatly increases our ability to evaluate the accuracy of $^{3}He_c$ and $^{21}Ne_c$ production rates and, therefore, $^{3}He_c$ and $^{21}Ne_c$ surface-exposure ages. Comparison of $^{3}He_c$ and $^{21}Ne_c$ age-pairs yielded by experimentally determined production rates and composition-based model calculations indicates that the former give more accurate surface exposure ages than the latter in this study. However, experimental production rates should be adjusted to the composition of the minerals being analyzed to obtain the best agreement between $^{3}He_c$ and $^{21}Ne_c$ ages for any given sample. $^{21}Ne_c/^{3}He_c$ values are 0.400 ± 0.029 and 0.204 ± 0.014 for olivine and pyroxene, respectively, in Bar Ten lava flows, in agreement with previously published values, and indicate that $^{21}Ne_c/^{3}He_c$ in olivine and pyroxene is not affected by erosion and remains constant with latitude, elevation, and time (up to 10 Myr). Samples with $^{21}Ne_c/^{3}He_c$ that do not agree with these values may indicate the presence of non-cosmogenic helium and/or neon. The neon three-isotope diagram can also indicate whether or not all excess neon in mineral separates comes from cosmogenic sources. An error-weighted regression for olivine defines a spallation line [$y = (1.033 \pm 0.031)x + (0.09876 \pm 0.00033)$], which is indistinguishable from that for pyroxene (Schäfer et al., 1999). We have derived a production rate of 25 ± 8 at/g/yr for $^{21}Ne_c$ in clinopyroxene (En_{43-44}) based on the $^{40}Ar/^{39}Ar$ age of the upper Bar Ten flow. Our study indicates that the production rate of $^{21}Ne_c$ in olivine may be slightly higher than previously determined. Cosmogenic ^{3}He and ^{21}Ne remain extremely useful, particularly when paired, in determining accurate eruption ages of young olivine- and pyroxene-rich basaltic lava flows.

1. Introduction

Cosmogenic ^{3}He and ^{21}Ne ($^{3}He_c$ and $^{21}Ne_c$) are produced predominantly by spallation reactions involving high-energy neutrons and target elements such as O, Na, Mg, Al, Si, Ca, and Fe (Lal, 1991; Gosse and Phillips, 2001; Niedermann, 2002). These noble gas nuclides are stable and accumulate over time and they are quantitatively retained in both olivine and pyroxene for up to 10 Myr (Cerling, 1990; Schäfer et al., 1999; Margerison et al., 2005). If a sample has experienced low or negligible erosion or burial, the amount of cosmogenic helium and neon in a sample directly equates to the amount of time that sample has been exposed to cosmic rays (Craig and Poreda, 1986; Kurz, 1986; Lal, 1987; Poreda and Cerling, 1992; Gosse and Phillips, 2001; Niedermann, 2002). $^{3}He_c$ and $^{21}Ne_c$ in olivine and pyroxene have been

used broadly to determine erosion rates and exposure ages of a variety of Quaternary surfaces including basalt flows, flood deposits, and associated desert pavements (e.g., Cerling, 1990; Poreda and Cerling, 1992; Laughlin et al., 1994; Wells et al., 1995; Schäfer et al., 1999; Fenton et al., 2001; 2002; 2004; Blard et al., 2005; 2007; Kounov et al., 2007; Gayer et al., 2008; Evenstar et al., 2009). Therefore, it is crucial that production rates of $^{3}He_{c}$ and $^{21}Ne_{c}$ in olivine and pyroxene be well established and as accurate as possible. Systematic cross calibration of production rates of different terrestrial cosmogenic nuclides was one of the main goals set by the CRONUS-EU research network, and was a driving force behind this study.

Production rates of $^{3}He_{c}$ and $^{21}Ne_{c}$ are derived from either experimental determinations on calibration sites of a known independent age (e.g., Poreda and Cerling, 1992; Cerling and Craig, 1994), or from experimental/numerical models that are based on the concentrations of major elements in minerals, particle fluxes in the Earth's atmosphere, and the cross-sections for relevant nuclear reactions associated with a given element (i.e., Lal, 1991; Masarik and Reedy, 1996; Schäfer et al., 1999; Masarik, 2002; Kober et al., 2005).

Production rates of $^{3}He_{c}$ in olivine and pyroxene are fairly similar because $^{3}He_{c}$ is produced mainly by O and Si, as well as Mg, Fe, and Ca. In contrast, though $^{21}Ne_{c}$ is mainly produced by Na, Mg, Al, and Si, there is no production of $^{21}Ne_{c}$ from O, so total production of $^{21}Ne_{c}$ in the same minerals is much less than that of $^{3}He_{c}$. Likewise, production of $^{21}Ne_{c}$ in olivine is higher than that in pyroxene, because olivine contains more Mg – one of the main target elements for the production of $^{21}Ne_{c}$ due to the high cross section of the reaction $^{24}Mg(n,\alpha)^{21}Ne$ (e.g., Masarik and Reedy, 1996; Schäfer et al., 1999; Niedermann, 2002). Though spallation reactions are the dominant production mechanisms for cosmogenic ^{3}He and ^{21}Ne, muon-

induced production of $^{3}He_c$ and $^{21}Ne_c$ must be considered, and can be significant at depth (Balco and Shuster, 2009). Data in this study, however, do not permit evaluation of the muon contribution, as samples were collected from the surfaces of young lava flows that do not appear to have been significantly affected by erosion. ^{3}He can also be produced in the $^{6}Li(n,\alpha)^{3}H(\beta^{-})^{3}He$ reaction, which is induced by thermalized neutrons resulting either from U/Th decay and subsequent (α,n) reactions within rocks or from the secondary cosmic ray cascade in the atmosphere and in rocks (Andrews and Kay, 1982; Lal, 1987; Dunai et al., 2007). Similarly, nucleogenic ^{21}Ne can be produced from $^{18}O(\alpha,n)^{21}Ne$ or $^{24}Mg(n,\alpha)^{21}Ne$ reactions and retained in olivine and pyroxene, and can be assessed based on the position of data in the Ne three-isotope diagram (Niedermann, 2002).

The Pleistocene Bar Ten lava mass is located in the western margin of the Uinkaret volcanic field in Grand Canyon National Park (AZ, USA; Figure 1). It was originally mapped as one lava flow (Hamblin, 1994; Fenton et al., 2001). During this study, we discovered that at least two flows make up the Bar Ten basalt. They are petrologically different (Figure 2) and are not easily distinguished in the field or in aerial photographs or maps. We refer to them here as the upper and lower Bar Ten flows, based on a change in petrology that occurs, and is obvious only in lab samples, about midway up the lava mass.

The Bar Ten flows are excellent sample sites for comparing the production of cosmogenic ^{3}He and ^{21}Ne in olivine and pyroxene phenocrysts because these minerals are abundant and in some cases coexisting. In addition, the flows have generally experienced little erosion due to a regional desert climate. These sites also give an opportunity to compare the reliability of composition-based production rates – rates

based on elemental concentrations in specific minerals – to experimentally calibrated production rates for the southwest USA.

The Bar Ten flows erupted some time before 80 ka based on a previously reported $^{3}He_{c}$ age (88 ± 6 ka; Fenton et al., 2001) and a thermoluminescence age of 108 ± 29 ka (Holmes et al., 1978). In the past, the presence of excess Ar, low K concentrations, and abundant glass in the lower basalt flow made it difficult to obtain a reliable $^{40}Ar/^{39}Ar$ age; there is one reported $^{40}Ar/^{39}Ar$ age of 190 ± 390 ka (Fenton et al., 2001). We report two new $^{40}Ar/^{39}Ar$ ages in this study — one age for each of the lower and upper flows.

In this paper, we present the results of $^{3}He_{c}$ and $^{21}Ne_{c}$ measurements and elemental analyses of olivine and pyroxenes collected from the informally named Bar Ten basalt flows (Fenton et al., 2001). With these data, we seek to address the following questions: (1) Do $^{3}He_{c}$ and $^{21}Ne_{c}$ concentrations for a given mineral sample yield the same surface exposure ages for a given nuclide-specific production rate? (2) Does the suite of cosmogenic nuclide concentrations for one lava flow reflect the age of this flow and does the age agree with the $^{40}Ar/^{39}Ar$ age of the same flow? (3) Are $^{21}Ne_{c}/^{3}He_{c}$ values constant with latitude, elevation, and time and do they agree with previously published values?

2. Methods

In this study, 12 samples for cosmogenic nuclide analysis were collected from stable, primary surfaces at elevations from 1180 to 1820 m above sea level along a vertical transect crossing both the lower and upper Bar Ten flows (Figure 3; Table 1). The vertical transect was essentially along a line of latitude, ranging from 36.2239° to 36.2417° N between 113.1889° and 113.2391° W. Eight samples (Figure 3; locales

"A-H") were collected from an olivine-basalt hereafter referred to as the lower Bar Ten flow, and four samples (Figure 3; locales "I-L") were collected from the upper Bar Ten flow, an olivine-pyroxene basalt. All four samples yielded pyroxene, but only one contained enough olivine for noble-gas analyses (250406-16). There is no obvious contact between the two flows in the field. In fact, the only distinguishing characteristic is the difference in petrology. This petrologic boundary between the two flows occurs somewhere between 1.34 and 1.65 km elevation (where samples 260406-20 and 051210-05 were collected, respectively). In addition, two samples for $^{40}Ar/^{39}Ar$ dating from each flow were collected at locales "B" and "I" (Table 1; Figure 3).

Samples for cosmogenic nuclide studies were collected from primary flow surfaces, such as the smooth level tops of pressure ridges and blisters (Figure 4) and rope structures preserved on tumuli (Figure 5). Skylines were measured with an inclinometer to account for topographic shielding of samples and samples were geographically located using GPS (WGS84 datum) and topographic maps (1:24,000). Samples were collected from locally high relief, thereby decreasing the possibility of burial or alluvial covering of sample surfaces. They were collected from surfaces that appeared to be stable and not affected by erosion.

Basalt samples were crushed, sieved and water-washed. Olivine and pyroxene minerals were concentrated from the 125-250 μm and 250-500 μm fractions (Table 1) using heavy-liquid and magnetic techniques. All olivine and pyroxene samples were examined under a binocular microscope and back-picked for purity. Data from both electron microprobe and ICP-AES analyses of the minerals indicate a high level of purity in the olivine and pyroxene separates (Table 2).

Olivine and pyroxene separates were analyzed for concentrations and isotopic compositions of all stable noble gases (except Kr and Xe isotopic compositions) in the noble-gas laboratory of GFZ Potsdam. Only results for helium and neon are shown and discussed in this paper. Three olivine samples and two pyroxene samples were crushed in vacuo to release and measure noble gases trapped in melt and fluid inclusions (Table 3). Only sample 250406-17 (pyroxene) was recovered from the crusher and later melted in the extraction furnace. All other samples were loaded into the furnace as phenocrysts, not powders. Olivine samples (0.25 to 1.65 g) and pyroxene samples (0.44 to 1.00 g) were wrapped in Al foil and placed in the sample carrousel above the extraction furnace, where they were baked under vacuum for about one week at 100°C. Noble gases were extracted in two or three heating steps up to 1750°C, in order to partly separate atmospheric and radiogenic from cosmogenic components (Table 3). All data have been corrected for analytical blanks, isobaric interferences, and mass discrimination effects. Error limits correspond to 95% confidence level and include analytical uncertainties. More details about the experimental procedure and the methods of data reduction can be found in Niedermann et al. (1997).

Aliquots of olivine and pyroxene that were analyzed for noble gases were also used for electron-microprobe and ICP-AES measurements at GFZ Potsdam. A minimum of 10 points within 2-6 individual grains of olivine or pyroxene for each sample were analyzed for Mg, Al, Si, Ca, Ti, Cr, Mn, Fe, and Ni content by electron microprobe. Approximately 300 mg of powdered olivine and pyroxene were used for ICP-AES determination of Na, Mg, Al, K, Ca, Ti, and Fe content. Powdered olivine and pyroxene were also used for ICP-MS determination of U, Th, and Li. Basalt JB-3 was used as a standard. Results for the standard were within 4, 3, and 2% of the

reported values for U, Th, and Li, respectively (Imai et al., 1995). REE concentrations for the two flows were determined with ICP-AES for whole-rock basalt samples from each flow.

2.1 REE patterns and $^{40}Ar/^{39}Ar$ ages

REE concentrations of two whole-rock basalt samples collected from the lower (051110-03) and upper (051210-04) lava flows, respectively, were measured on the GFZ Potsdam ICP-AES and are shown in Figure 2. Results for the basalt standard BM measured in the same run were withing 20% of the reported values (Govindaraju, 1994). All REE values are normalized to chondrite values reported in Taylor and McClennan (1985) (Figure 2).

Both the lower and upper Bar Ten lava flows are alkali-olivine basalts, but the REE data from the upper flow (sample 051210-04) shows additional enhancement in light REE concentrations. Sample 051210-04 has a higher La/Gd ratio of 4.3 compared to that of sample 051110-03 (La/Gd = 3.1). The REE data, in combination with the mineralogical nature and $^{39}Ar/^{40}Ar$ ages reported here for the upper and lower Bar Ten flows, quantitatively show that the lava flows are distinct from one another.

Two $^{40}Ar/^{39}Ar$ samples were collected from the same locations as the REE samples – one from the lower flow (sample 051110-02), one from the upper flow (sample 051210-05) – and were prepared and analyzed in accordance with methods described in Koppers et al. (2000) and Schneider et al. (2009; this issue)**.** For $^{40}Ar/^{39}Ar$ analysis, the basalt samples were crushed and the 500-1000 μm fraction was washed, dried and handpicked to exclude phenocryst-bearing grains. Only groundmass from each sample was analyzed. Approximately 1 g of groundmass from each sample were

wrapped in aluminum foil and stacked in a 22-mm diameter quartz glass cylinder together with DRA-1 sanidine internal laboratory standards and sent for a 1h irradiation in the RODEO facility in the ECN HFR nuclear reactor in Petten (Netherlands).

After return and a cool down period to let the ^{37}Ar activity of the sample decrease to safe levels, the samples were mounted in the metal revolver sample holder of the AGES facility in the noble gas laboratory in the Faculty of Earth and Life Science at the Free University Amsterdam. Each sample was dropped into the furnace the day before measurement and baked over night at 500 ºC. ^{40}Ar/^{39}Ar incremental heating experiments were undertaken in the temperature range between 700 ºC and 1200 ºC using 11 steps for sample 051210-05 and 9 steps for sample 051110-02.

Despite a thorough bake-out at 500 ºC, both samples showed very low enrichment in radiogenic isotopes (~50% blank contributions in some steps) and high trapped air content (<1% of the ^{40}Ar signal is radiogenic). The large amount of trapped air even in high temperature steps and the uncertainties of the blanks (~ 2.5% for ^{40}Ar over the whole temperature range) made it difficult to obtain accurate ages. In addition, isochrons and inverse isochrons of the measurements are ill defined due to the high enrichment in air.

As a result, sample 051110-02 (lower flow) shows concordant plateau, isochron and total fusion ages. Sample 051210-05 (upper flow) shows concordant plateau and total fusion ages, and both normal and inverse isochron ages agree (within high 1σ error) but are lower than plateau and total fusion ages (see Supplementary Data). In summary, samples 051110-02 and 051210-05 yield plateau ^{40}Ar/^{39}Ar ages of 117 ± 32 and 80 ± 25 ka, respectively. These ages are not significantly different, as they overlap within uncertainties, and they are consistent with a published

thermoluminescence (TL) age of 108 ± 29 ka (Holmes et al., 1978). Holmes et al. (1978) do not report an exact location for the TL sample. If it was collected near the one dirt road that exists on the Bar Ten lava mass, it was likely derived from what we informally call the lower Bar Ten flow.

Despite the overlapping uncertainties, the $^{40}Ar/^{39}Ar$ ages support petrologic evidence in this study that the Bar Ten lava mass is made up of two lava flows that are stratigraphically indistinguishable and whose eruption ages are very similar. The noticeable difference in the mineralogy of the basalts is the presence of both pyroxene and olivine phenocrysts in samples collected at and above an elevation of 1.48 km; below this elevation, basalts only yielded olivine phenocrysts. According to the nominal $^{40}Ar/^{39}Ar$ ages, the sample collected on the lower flow at an elevation of 1.18 km (051110-02; locale "B" in Figure 3a) is older than the sample collected on the upper flow at locale "I" at an elevation of 1.65 km (051210-05; Figure 3a). Though the $^{40}Ar/^{39}Ar$ age of the upper Bar Ten flow has an uncertainty of 32%, this independent age yields an opportunity to give the first estimate of a calibrated production rate for $^{21}Ne_c$ in clinopyroxenes.

3. He and Ne Results

3.1. Interlaboratory comparison

Cosmogenic noble gas measurements of olivine and pyroxene in basalts of the Uinkaret volcanic field have been undertaken for different studies in three different laboratories: the University of Rochester, the University of Utah, and now the GFZ Potsdam. Fenton et al. (2001; 2002; 2004) demonstrated that replicate analyses of $^{3}He_c$ in labs at the Universities of Rochester and Utah were consistent and therefore data between the labs could be compared in their studies.

In this project, we measured noble gases at GFZ Potsdam in olivine sample 97-AZ-330-BT (sample locale "F", Figure 3a), which was collected in 1997 and initially analyzed at the University of Rochester during a previous study of the Uinkaret volcanic field lavas (Fenton et al., 2001). At the University of Rochester, olivine phenocrysts were pre-crushed to a fine powder before analysis, to decrease the influence of helium present in fluid inclusions on the measurement. An aliquot of the same olivine phenocrysts of size 250-500 μm was analyzed without prior crushing at the GFZ Potsdam. The resultant ^3He_c concentrations measured during melting in the furnace in crushed and uncrushed olivine are identical within error limits (Table 1; Figure 6). We conclude that partial release of ^3He_c due to preliminary crushing (Blard et al., 2006) does not affect data reported in Fenton et al. (2001; 2002; 2004) and may only be a concern in this study for sample 250406-13 (pyroxene), whose crush $^3He/^4He$ value was 29 +36/-29 R_a. Likewise, the only sample from this study that was recovered from the crusher and used as a fusion sample in the furnace at GFZ Potsdam (250406-17 pyroxene) showed a crush $^3He/^4He$ ratio of 15.2 ± 7.3 R_a. It is noted, however, that pyroxene crushes yielded ^4He concentrations two orders of magnitude lower than those of crushed olivine and therefore the uncertainty on the sample -13 measurement is >100%. It appears that pyroxene contains less magmatic He than olivine, and thus the ^4He extracted by heating may have a larger component of radiogenic ^4He. This is supported by the calculation of predicted radiogenic ^4He in olivine and pyroxene based on U and Th concentrations and equations by Andrews (1985) (Table 4). Thus, the evidence for release of cosmogenic He by crushing is weak, and helium data from this study can be directly compared to that published in Fenton et al. (2001; 2002; 2004).

Data from sample 97-AZ-330-BT and other samples collected in 1997 are plotted

in Figure 6a (dashed ellipse) and listed in Table 1. Here, the data are calculated using a magmatic $^{3}He/^{4}He$ value of 6.06 ± 0.46 R_a (section 3.2) to correct for contributions from trapped gases. In their original form, reported in Fenton et al. (2001), the data were corrected with a magmatic $^{3}He/^{4}He$ value of 7.22 R_a, with $^{3}He_c$ concentrations that were 0.04-0.64% lower than those reported here for the same samples. However, the data reported here for the 1997 samples (Table 1) still show comparable or even lower $^{3}He_c$ concentrations than samples collected at lower elevations in 2006. Samples from the same lava flow at higher elevations should yield higher cosmogenic isotope concentrations though. We believe that the low $^{3}He_c$ concentrations, particularly those in sample 97-AZ-330-BT, reflect thin slab- or block-erosion of the tumuli from which the samples were collected. Sample sites from 1997 are located near the active Hurricane Fault (locales A, F, and G; Figure 3), where surface ruptures have occurred (Fenton et al., 2001). It is possible that loose tops on tumuli near fault scarps could have been "shaken loose" during fault ruptures. The loss of any surface material would cause an apparent "loss" of cosmogenic nuclides, and thus younger surface exposure ages. This conclusion is supported by the low $^{21}Ne_c$ concentration of sample 97-AZ-330-BT (Fig. 6b).

3.2 In vacuo crush analyses

Five samples were crushed at GFZ Potsdam to determine the isotopic composition of trapped noble gases; three samples were olivine, two were pyroxene (Table 3). Helium gas in olivine yielded an average $^{3}He/^{4}He$ value of 6.06 ± 0.46 R_a. As previously discussed, the pyroxene samples -13 and -17 yielded $^{3}He/^{4}He$ values of 29 +36/-29 and 15.2 ± 7.3 R_a, respectively. Despite the large uncertainties, these values are considerably higher than other mantle gas values for the Bar Ten or other lava flows within the same volcanic field (Fenton et al., 2001; 2002; 2004). In the absence

of a "good" crush measurement for the Bar Ten pyroxenes, the average olivine crush $^{3}He/^{4}He$ value of 6.06 ± 0.46R_a is used to account for trapped gases in both olivine and pyroxene.

In vacuo crushing of two olivine samples and two pyroxene samples yielded fluid-inclusion gases with $^{22}Ne/^{20}Ne$ and $^{21}Ne/^{20}Ne$ values that were indistinguishable from the values of air within the uncertainties of the measurements (Figure 7). One crush sample (240406-08) yielded an enhanced $^{21}Ne/^{20}Ne$ value of 0.322±0.010 that did not overlap that of air, indicating the presence of mantle neon in this olivine.

3.3 Concentrations of $^{3}He_c$ and $^{21}Ne_c$

Three main sources contribute to the total helium and neon inventories in a volcanic rock: (1) trapped, (2) radiogenic/nucleogenic, and (3) cosmogenic components (Mamyrin and Tolstikhin, 1984). Trapped components may be atmospheric, magmatic (i.e., mantle-derived), or possibly crustal in their origin. Concentrations of $^{3}He_c$ and $^{21}Ne_c$ in young basalts (i.e., <500 ka) with negligible U, Th, and Li contents are obtained by using the following equations (Niedermann, 2002):

$$^{3}He_c = \left[\left(^{3}He/^{4}He\right)_{meas} - \left(^{3}He/^{4}He\right)_{tr}\right] \times {}^{4}He_{meas} \quad [1]$$

$$^{21}Ne_c = \left[\left(^{21}Ne/^{20}Ne\right)_{meas} - \left(^{21}Ne/^{20}Ne\right)_{tr}\right] \times {}^{20}Ne_{meas} \quad [2]$$

where the subscripts *c*, *meas*, and *tr* mean cosmogenic, measured, and trapped. Trapped helium usually has a mantle isotopic signature and trapped neon is usually atmospheric in isotopic composition (Niedermann, 2002). Trapped gas ratios are determined, as discussed above, by crushing samples in vacuo.

3.4 Cosmogenic ^{3}He

Helium isotope data are listed in Tables 1 and 3 and are illustrated in Figure 6a. The $^{3}He_{c}$ concentrations in Table 1 and Figure 6a are corrected for self- and topographic shielding. In the lower Bar Ten flow, excluding the samples taken by Fenton et al. (2001) in 1997, concentrations of $^{3}He_{c}$ in olivine range from 25.8±1.3 to 29.7±1.2 Mat/g (Mat = million atoms). Pyroxenes and one olivine in the upper flow yielded $^{3}He_{c}$ concentrations ranging from 35.2±2.8 to 39.3±2.8 Mat/g. Though the upper flow is petrologically distinct and seemingly younger than the lower flow (based on insignificantly different $^{40}Ar/^{39}Ar$ ages), the overall pattern of $^{3}He_{c}$ along the sampling transect across both flows increases with elevation, appearing to indicate the flows are very similar in age.

Samples collected at the same locale are expected to yield similar cosmogenic nuclide concentrations, assuming the landform surface has had the same erosion/burial history for that site. Five basalt samples were collected in two different locations on the lower Bar Ten flow (sample locales "B and C"; Figure 3a). These samples only yielded olivine for analyses. Group B includes samples 051110-01 and -03 and Group C includes samples 240406-06, -08, and -09. Groups B and C were collected from two different pressure ridges approximately 600 m apart at roughly the same elevations (~1.18 km). Each group of samples was collected from continuous flat, horizontal surfaces on top of separate pressure ridges (Figure 4b). The samples in each group were collected within 2 m of one another. The pressure-ridge surfaces have well-developed desert varnish and a smooth, very resistant massive surface made of glassy olivine-rich basalt (Figure 4); pahoehoe and aa features are absent. There is no obvious evidence of erosion or exfoliation of the surfaces that were sampled. The pressure ridge surfaces are several meters above the surrounding area of the lava flow, thus minimizing the possibility of burial by ash or local alluvium.

The major-element compositions of the olivine separates from Groups B and C are indistinguishable with forsterite contents ranging from Fo_{81}-Fo_{82} based on microprobe analyses (Table 2).

Similar elevation, sample locale, sample type, and olivine composition indicate that all five olivine samples should yield very similar $^{3}He_c$ and $^{21}Ne_c$ concentrations in the absence of erosion/burial and on the basis that they are from the same lava flow. Likewise, the $^{21}Ne_c$ /$^{3}He_c$ values for all these olivines should be similar, particularly because the ratio is theoretically unaffected by erosion/burial, and because the nuclides form at a constant rate relative to one another over time and geographic position unless the contributions by muogenic production are significant and substantially different for the two nuclides.

Indeed, the $^{21}Ne_c$ concentrations agree well within and between the groups and range from 10.35 ± 0.77 to 11.15 ± 0.76 Mat/g including corrections for shielding. Technical difficulties were experienced during the helium analyses of samples 051110-03 and 240406-09 (as well as 240406-10 from locale A), and no $^{3}He_c$ concentrations were determined for these samples (Table 1). $^{3}He_c$ concentrations for samples 051110-01, 240406-06, and 240406-08 vary from 25.8±1.3 to 29.7±1.2 Mat/g. Samples -06 and -08 are from the same sample site, but their $^{3}He_c$ concentrations do not overlap within their uncertainties; however, their $^{21}Ne_c$ concentrations do agree and tend to rule out differing amounts of erosion. Therefore, it is unlikely that sample -06 has "lost" any $^{3}He_c$, but it is possible that sample -08 contains additional ^{3}He that is not accounted for in our calculations. Such an additional ^{3}He component in olivine and pyroxene can be magmatic or nucleogenic, or can be produced by cosmogenic thermal neutrons (Dunai et al., 2007).

^{3}He can be produced in the ^{6}Li(n,α)^{3}H(β^{-})^{3}He reaction, which is induced by thermalized neutrons resulting either from (α,n) reactions following U/Th decay within rocks (Andrews and Kay, 1982; Lal, 1987) or from the secondary cosmic ray cascade in the atmosphere and in rocks (Dunai et al., 2007). Both production paths can significantly contribute to the total ^{3}He system in rocks with high Li concentrations. Basalts typically have low Li content. Mantle-derived high-Mg basalts (MgO > 4%) typically contain only 5 ± 2 ppm Li (Chan and Frey, 2003; Ryan and Kyle, 2004) and Li-concentrations in olivine and pyroxene are usually even smaller (Brenan et al., 1999; Ryan and Kyle, 2004; Seitz et al., 2004). In this study, Li contents range from 2.1 to 5.0 ppm in pyroxene and from 2.4 to 3.6 ppm in olivine from both the upper and lower Bar Ten lava flows (Table 2). Based on these U, Th, and Li concentrations and the equations of Andrews (1985), we expect <0.001% of the total measured ^{3}He in our samples to be of nucleogenic origin as a result of the ^{6}Li(n,α)^{3}H(β^{-})^{3}He reaction (Table 4). Futhermore, implantation of ^{3}He produced by thermalized neutrons in the same reaction in surrounding minerals should be negligible in our samples because the phenocrysts (prior to crushing) are large (>500 μm) relative to the ejection distance (~30 μm) of the nucleogenic ^{3}He (Dunai et al., 2007) and Li concentrations are low.

Similarly, calculated $^{3}He_{c}$ contents can seem "too low" if the measured ^{4}He in a melted olivine or pyroxene contains radiogenic ^{4}He that is not accounted for, produced either in the surrounding rock matrix and injected into the mineral of interest or in that mineral itself (Blard and Farley, 2008). Still, this effect does not appear to explain the low $^{3}He_{c}$ concentration in sample -06. Samples -06 and -08 contain similar total ^{4}He contents of 146.6 and 139.9 Gat/g (billion atoms per gram). Based on their respective U and Th concentrations (0.03-0.05 ppm and 0.05-0.10

ppm, respectively; Table 4) and an estimated eruption age of 95 ka, 23 and 13 Gat/g of ^{4}He would accumulate within the olivine crystals during that time. This equals 15% and 9% of total measured ^{4}He in olivine samples -06 and -08, respectively. Furthermore, the ejection distance of radiogenic ^{4}He is ~20 µm (Ziegler, 1977), and phenocrysts in this study are >500 µm prior to crushing, so significant implantation of ^{4}He is also unlikely. U and Th values were not determined for the groundmass in Bar Ten lava flows. Using mean U and Th values of 2.3 and 6.1 ppm for basalts and andesites (Blard and Farley, 2008), and an estimated 5% of ejected alpha particles that are retained in surrounding minerals with diameters >500 µm (Farley et al., 1996), only 3% of the total ^{4}He measured in our olivine samples is likely due to implantation and is small compared to radiogenic ^{4}He that would accumulate within olivines/pyroxenes. Correcting for the presence of radiogenic/nucleogenic helium in our samples indicates that there are apparent increases of cosmogenic ^{3}He concentrations in olivines and pyroxenes of <0.9% and <2%, respectively (Tables 1 and 4). This causes no significant change to $^{3}He_{c}$ exposure ages in olivine and a 1-5% increase in ^{3}He exposure ages in pyroxene. This all suggests that the effects of implanted radiogenic ^{4}He and the contribution of nucleogenic and thermal neutron-produced cosmogenic ^{3}He are negligible in olivines, but should be considered in pyroxenes, in our study.

3.5 Neon Three-Isotope Diagram and Determination of $^{21}Ne_{c}$

Neon isotope data are listed in Tables 1 and 3 and are illustrated in Figure 6b. The $^{21}Ne_{c}$ concentrations in Table 1 and Figure 6b are corrected for self- and topographic shielding.

Neon analyses in olivine can be used to determine the spallation line for this mineral in the neon three-isotope diagram (Figure 8a). An error-weighted regression

defines a spallation line [y = (1.033 ± 0.031)x + (0.09876 ± 0.00033)] through our olivine data, which is, within uncertainties, indistinguishable from the line for pyroxene (Schäfer et al., 1999). All data points fall within error limits onto either the olivine or pyroxene spallation lines (Figures 8a and 8b). Both spallation lines pass very closely through the atmospheric point on the lower left, indicating that apart from minor contributions of mantle Ne, the olivine and pyroxene samples contain only atmospheric and cosmogenic neon (Niedermann, 2002).

In the lower Bar Ten flow, concentrations of $^{21}Ne_c$ range from 10.08±0.65 to 12.32±0.76 Mat/g in olivine (again excluding the sample collected in 1997). Pyroxenes in the upper flow yielded $^{21}Ne_c$ concentrations ranging from 7.27±0.50 to 7.87±0.87 Mat/g, and the one olivine sample in the upper flow had 15.7±1.2 Mat/g. There is a general increase in $^{21}Ne_c$ in olivine with increasing elevation (Figure 6b), excluding sample 97-AZ-330-BT, which was affected by erosion, as previously discussed. $^{21}Ne_c$ concentrations in pyroxenes appear to be relatively constant between 1.6 and 1.8 km (200 m elevation gain), but it is possible that sample -13 experienced a slight amount of erosion.

3.6 $^{21}Ne_c/^{3}He_c$

The $^{21}Ne_c/^{3}He_c$ ratio for Bar Ten olivine varies from 0.349±0.030 to 0.432±0.037 with an average and standard deviation of 0.400 ± 0.029 (Figure 9). This average value is consistent with the $^{21}Ne_c/^{3}He_c$ value of 0.41 ± 0.05 reported for olivine in lava flows less than 25 ka by Poreda and Cerling (1992). Poreda and Cerling (1992) analyzed Fo_{74-87} olivines and the Bar Ten flows contain Fo_{77-84} olivines, i.e. the chemical compositions in the two studies overlap. Bar Ten clinopyroxene (En_{43-44}) yields a lower average $^{21}Ne_c/^{3}He_c$ value (0.202 ± 0.014; Figure 9) than that of Bar Ten olivines. This is expected because pyroxenes contain approximately one-third as

much Mg as olivine, along with only modestly higher Si and Al contents, and 98% of $^{21}Ne_c$ is produced through spallation reactions involving these three elements (Schäfer et al., 1999). Poreda and Cerling (1992) report a similar $^{21}Ne_c/^{3}He_c$ value of 0.222 ± 0.016 for one pyroxene sample (En_{44}). Our $^{21}Ne_c/^{3}He_c$ data are consistent with that of Poreda and Cerling (1992), Schäfer et al. (1999) and Niedermann et al. (2007), and all data taken together show that the ratios in olivine and pyroxene do not appear to change with elevation (from 1180 to 1820 m), latitude, or time for the past 10 Ma. There is some change with chemical composition, but the difference falls within uncertainties of measurements.

3.7 Microprobe and ICP-AES Data

Data from both microprobe and ICP-AES analyses indicate that our mineral separates were very pure (Table 2). Based on microprobe data, olivines in this study range from Fo_{80} to Fo_{84}, with one sample (240406-10) yielding an average content of Fo_{77}. On average, olivines contain 26.4 wt.% Mg and 12.4 wt.% Fe. Clinopyroxenes in this study yield an average content of $En_{43\text{-}44}$ and contain on average 9.8 wt.% Mg, 4.6 wt.% Fe, 15.3 wt.% Ca, and 1.9 wt.% Al.

4. Production Rates

We use the cosmogenic nuclide data from our study to calculate and compare exposure ages derived from (1) experimentally determined production rates for $^{3}He_c$ and $^{21}Ne_c$ in olivine (Poreda and Cerling, 1992; Cerling and Craig, 1994) and pyroxene (this study) and (2) compositional-based production rates derived using the model calculations of Masarik (2002) and Kober et al. (2005). Independent age-dating of the Bar Ten lava flow (i.e. $^{40}Ar/^{39}Ar$ and thermoluminescence techniques) is not accurate enough to calibrate a production rate from $^{3}He_c$ and $^{21}Ne_c$ measurements in

this study; however, we do estimate a production rate for $^{21}Ne_c$ in clinopyroxene based on our noble gas data and the $^{40}Ar/^{39}Ar$ age of the upper Bar Ten flow.

4.1 Experimental production rates

We choose to evaluate the experimentally calibrated $^{3}He_c$ and $^{21}Ne_c$ production rates of Cerling and Craig (1994) and Poreda and Cerling (1992), respectively, for three reasons. Firstly, Licciardi et al. (2006) emphasize the usefulness of choosing a production rate whose calibration site has a geographic location and elevation similar to that of the study site of interest. Tabernacle Hill is the calibration site for experimentally determined production of $^{3}He_c$ and $^{21}Ne_c$ in olivine and it is located at 1455 m elevation in southern Utah, just 3° north of the Bar Ten flow (Poreda and Cerling, 1992; Cerling and Craig, 1994). Secondly, $^{3}He_c$ exposure ages reported in Fenton et al. (2001; 2002; 2004) were calculated using Cerling and Craig's (1994) production rate of 115 ± 4 at/g/yr (for Fo_{81} olivine). Using the same Cerling and Craig (1994) $^{3}He_c$ production rate here allows for the inter-comparison of data among Fenton et al. (2001; 2002; 2004) and this study. Thirdly, Tabernacle Hill olivine is the only olivine used in an experimental calibration study that has reported $^{3}He_c$ and $^{21}Ne_c$ concentrations. To the best of our knowledge, no other study has evaluated the accuracy of the production of $^{21}Ne_c$ in olivine.

Scaling factors play an important role in determining production rates at any given site, and there are several schemes from which to choose, e.g. Lal (1991), Dunai (2000), and Stone (2000), to name a few. Fenton et al. (2001; 2002; 2004) used the scaling factors of Lal (1991), so, for the sake of simplicity and consistency, we scale all production rates in this study with Lal's (1991) scaling factors as derived by CosmoCalc (http://cosmocalc.googlepages.com; Vermeesch, 2007). Resulting $^{3}He_c$ and $^{21}Ne_c$ production rates in olivine (Fo_{81}) are 118 ± 4 and 45 ± 4 at/g/yr,

respectively. The ^{3}He production rate of 115 ± 4 at/g/yr originally reported by Cerling and Craig (1994) is based on cosmogenic data from Tabernacle Hill samples in addition to other western USA calibration sites and was scaled to high-latitude, sea-level using T. Cerling's fit to Lal's (1991) data (pers. comm., T. Cerling, 2007). Cerling's scaling factors are 2-3% higher than those calculated by CosmoCalc, thus the conversion from 115 to 118 at/g/yr in this study. The ^{3}He rate is consistent with the overall mean $^{3}He_c$ production rates reported for the western USA (Licciardi et al., 2006), using scaling methods of Lal (1991), Stone (2000), and Dunai (2000).

4.1.1 Estimated $^{21}Ne_c$ production rate in pyroxene

To the best of our knowledge, there is no published experimental determination of the $^{21}Ne_c$ production rate in clinopyroxene. Though the independent age-dating of the Bar Ten lava flow does not allow an accurate calibration in this study, we can at least provide an estimate of the $^{21}Ne_c$ production rate in clinopyroxene based on the $^{40}Ar/^{39}Ar$ age of the upper lava flow, where the samples yielding pyroxene were collected. Table 5 lists an estimated average production rate of 25±8 at/g/yr, which is determined by dividing the measured concentrations of $^{21}Ne_c$ in our pyroxene samples (Table 1) by the $^{40}Ar/^{39}Ar$ age of 80 ± 25 ka of the flow and scaling to high-latitude and sea-level using Lal (1991) in CosmoCalc (Vermeesch, 2007). The uncertainty of our estimated production rate is 32%, which is mainly due to the $^{40}Ar/^{39}Ar$ age uncertainty but also includes the $^{21}Ne_c$ analytical uncertainty (Table 5).

4.2 Production rates based on mineral composition

Compositional production rates are based on the total sum of elemental production rates for a given mineral, such as olivine or pyroxene (Lal, 1991; Masarik, 2002; Kober et al., 2005). Because major-element concentrations vary within and between minerals, it is logical that production rates of $^{3}He_c$ and $^{21}Ne_c$ will also vary, even if

only slightly. We measured major-element concentrations in olivine and pyroxene from the upper and lower Bar Ten flows using an electron microprobe and elemental ICP-AES bulk-sample analyses.

Production rates in this study derived from the model calculations of Masarik (2002) and Kober et al. (2005) are based on the compositions of Bar Ten olivine (Fo_{77-84}) and pyroxenes (En_{43-44}) within the mineral structures [$(Mg, Fe)_2SiO_4$] and [$(Ca, Mg, Fe)(Si, Al)O_3$], respectively. Molar fractions of Mg and Fe vary based on their concentrations in any given olivine, whereas Si and O molar fractions are fixed at 1 and 4, respectively. Ca, Mg, and Fe hold places in the cation position in clinopyroxene and molar fractions vary according to the concentrations. Likewise, Al and Si substitute for one another in the $(Si,Al)O_3$ structure; the molar fraction of O is fixed at 3 in this case. Production rates can be calculated using these mineral structures, elemental concentrations, and Eqs. 3 and 4 as follows:

$$\frac{\left[\left(X_{Mg} * A_{Mg} * P_{Mg}\right) + \left(X_{Fe} * A_{Fe} * P_{Fe}\right) + \left(1 * A_{Si} * P_{Si}\right) + \left(4 * A_{O} * P_{O}\right)\right]}{W} = P_M, \quad [3]$$

and

$$\frac{\left[\left(X_{Ca} * A_{Ca} * P_{Ca}\right) + \left(X_{Mg} * A_{Mg} * P_{Mg}\right) + \left(X_{Fe} * A_{Fe} * P_{Fe}\right) + \left(X_{Si} * A_{Si} * P_{Si}\right) + \left(X_{Al} * A_{Al} * P_{Al}\right) + \left(3 * A_{O} * P_{O}\right)\right]}{W} = P_M \quad [4]$$

where X_i is the molar fraction of element i (Mg, Fe, Ca, etc.); A_i is the atomic mass (g/mol); P_i is the production rate of ^3He_c or $^{21}Ne_c$ from the respective element; P_M is the total production rate (at/g/yr), for either ^3He_c (P_{M3He}) or $^{21}Ne_c$ (P_{M21Ne}); and W is the molecular weight (g/mol) of the mineral of interest. Additional cation elements (Table 2) are present in trace amounts in olivine and pyroxene, but have negligible effects on calculation of production rates.

Production rates based on microprobe elemental analyses are within 0.2 to 2.8% of those calculated using elemental ICP-AES bulk-sample analyses. This indicates that either analytical technique is accurate for methods derived by Masarik (2002) and Kober et al. (2005), despite the expectation that point-analyses with a microprobe may bias elemental concentration data by not representing variations in mineral composition due to zoning. Only compositional production rates based on microprobe data are discussed below and are listed in Table 6.

5. Exposure Ages

5.1 Comparison of $^{3}He_c$ and $^{21}Ne_c$ exposure ages based on different production-rate methods

In principle, samples collected at the same site on a lava flow are expected to yield similar $^{3}He_c$ and $^{21}Ne_c$ ages, when comparing sample to sample, for olivine or pyroxene. Ideally, all samples from the same lava flow would behave similarly, assuming the entire surface has had the same geomorphic (i.e., erosion/burial) history. Samples 250406-15 and -16 were both collected from the same site (Figure 3) on the upper Bar Ten flow and yield cosmogenic nuclide data that strongly agree between samples in olivine and pyroxene. This sample set is ideal for evaluating the accuracy of the production rates discussed above.

Samples 250406-15 and -16 were both collected from ropy, pahoehoe structures on a tumulus on the upper half of the Bar Ten flow. The ropy structures were resistant to hammering and indicated no obvious evidence of erosion. There was a slight depression to the surface, which was higher than the surrounding lava flow, so it is possible that ash from subsequent eruptions may have temporarily covered the surface; however, both samples were collected on the same continuous surface within

2 m of each other, so they should have experienced these processes in the same manner. Both samples yielded clinopyroxene and sample -16 also contained enough olivine for analyses.

Cosmogenic ^{3}He contents in the pyroxene and olivine from sample -16 agree within error limits, although the concentration is nominally higher in the pyroxene (Table 1). Sample -15 pyroxene yields a slightly lower $^{3}He_c$ content than that of sample -16 pyroxene and -16 olivine, but all $^{3}He_c$ contents still agree within uncertainties (Figure 6; Table 1). This might indicate that sample -15 underwent some erosion/burial that sample -16 did not, however, samples -15 and -16 pyroxenes have similar $^{21}Ne_c$ concentrations, and sample -15's $^{21}Ne_c$ value is even slightly higher (7.87 ±0.87 and 7.66 ±0.55 Mat/g, respectively). The olivine from sample -16 yielded a $^{21}Ne_c$ concentration (15.7 ± 1.2 Mat/g) double that of $^{21}Ne_c$ in the pyroxenes; however, this is expected, as production of $^{21}Ne_c$ increases with increasing Mg content and olivine contains more Mg (Poreda and Cerling, 1992).

Based on agreement in nuclide concentrations, samples -15 (pyroxene), -16 (pyroxene), and -16 (olivine) should yield identical $^{3}He_c$ and $^{21}Ne_c$ age-pairs for each mineral if production rates are accurate and each age-pair should fall on a 1:1 line (within error limits) when graphed (Figure 10). Ideally, all exposure ages would agree within error, and would all fall on one point on the 1:1 line. Nuclide concentrations are taken from Tables 1 ($^{21}Ne_c$ values) and 4 ($^{3}He_c$ values).

$^{3}He_c$ and $^{21}Ne_c$ age-pairs for samples -15 (pyroxene), -16 (olivine), and -16 (pyroxene) are calculated using 3 production rate schemes: (1) experimentally calibrated production rates in olivine (118 and 45 at/g/yr; Cerling and Craig, 1994; Poreda and Cerling, 1992) and our estimated calibrated $^{21}Ne_c$ production rate in pyroxene (25±8 at/g/yr); (2) compositional production rates determined with model

calculations of Kober et al. (2005); and (3) compositional production rates determined with model calculations of Masarik (2002). Exposure ages are graphed in Figure 10a and shown as the Calibrated, Kober, and Masarik age groups, indicated by ellipses.

The Calibrated age group is the only group whose ages all agree within error with each other and whose ages fall closest to or on the 1:1 line. This indicates that production rates calibrated by Cerling and Craig (1994) and Poreda and Cerling (1992) remain accurate for olivine and pyroxene in the southwest USA, even before accounting for differences in chemistry. Figure 10a also shows that our estimated $^{21}Ne_c$ production rate of 25 at/g/yr in clinopyroxene produces correct ages within analytical uncertainties, even without taking into account the 32% systematic uncertainty of the production rate.

The Masarik group shows good internal agreement of all three age-pairs, with very similar $^{21}Ne_c$ ages and overlapping $^{3}He_c$ ages for all three samples. $^{3}He_c$ ages in the Masarik group are 9-14% higher than those in the Calibrated group when comparing the same sample in each group. $^{21}Ne_c$ ages in the Masarik group are 11-17% lower than those in the Calibrated group. There is also some overlap in age-agreement including uncertainty between the Calibrated and Masarik groups; however, none of the samples in the Masarik group fall on the 1:1 line. It appears that $^{3}He_c$ production rates are too low and/or $^{21}Ne_c$ production rates are too high using Masarik's (2002) production-rate method.

The Kober group has one sample falling on the 1:1 line and strong internal agreement in $^{21}Ne_c$ ages between the two pyroxene samples; however, samples -16 (olivine) and -16 (pyroxene) have very different $^{3}He_c$ and $^{21}Ne_c$ ages that do not agree even within error limits. Overall, $^{3}He_c$ ages and $^{21}Ne_c$ ages are 13-28% and 22% lower than those in the Calibrated age group when calculated using production rates from

Kober et al.'s (2005) method. It is noted that $^{21}Ne_c$ ages in the Kober group are only 7-13% lower and overlap those in the Masarik group within error. Dunai et al. (2007) discuss discrepancies in Kober et al.'s (2005) model in more detail and suggest that anomalously high $^{3}He_c$ production rates may be due to excess implanted ^{3}He from cosmogenic thermal neutron production that was present in the samples.

Based on our sample set and the age-pairs yielded by the three different production-rate methods, we conclude that the calibrated production rate method remains the most accurate for this region of the USA. However, it can be improved by correcting for differences in elemental concentrations. Hereafter, all corrections relating to variations in chemistry follow the normalization of Masarik's (2002) scheme to production rates for $^{3}He_c$ and $^{21}Ne_c$ in the Tabernacle Hill flow. For example, the olivine from Tabernacle Hill (Poreda and Cerling, 1992) is Fo_{81}, whereas Bar Ten olivine ranges from Fo_{77}-Fo_{84}. Hypothetically, production rates of $^{3}He_c$ and $^{21}Ne_c$ should be lower or higher in Bar Ten olivine than in Tabernacle Hill olivine, because there is less or more Mg (i.e. variable forsterite content). In the case of sample -16 olivine, the production rate is slightly higher, because of a higher Mg content than thatof Tabernacle Hill olivine.

5.2 Composition-corrected production rates and related exposure ages

To correct for differences in elemental concentrations, compositional-based production rates for Bar Ten olivine (Fo_{77} to Fo_{84}) and pyroxene (En_{43-44}) were normalized to calibrated production rates of 118 and 45 at/g/yr for $^{3}He_c$ and $^{21}Ne_c$ in olivine (Fo_{81}; Cerling and Craig, 1994; Poreda and Cerling, 1992) using Masarik (2002) elemental production rates (Tables 6 and 7).

First, Masarik's (2002) elemental production rates are normalized to experimentally calibrated production rates for Fo_{81}. To do so, P_{3Hec} and P_{21Nec} predicted by Masarik's (2002) model are calculated for the chemical composition Fo_{81} (25.8% Mg, 13.9% Fe, 18.4% Si, 41.9% O) using Eq. 3. Normalization factors are calculated by dividing the experimentally calibrated rates by P_{M3He} and P_{M21Ne}:

$$\frac{118\ (\text{at/g/yr})}{P_{M\,3He}} = 1.099 \text{ and } \frac{45\ (\text{at/g/yr})}{P_{M_{21Ne}}} = 0.851 \quad .$$

These normalization factors indicate that Masarik's (2002) model underestimates the element-specific production rates of $^{3}He_c$ by ~10% and overestimates those of $^{21}Ne_c$ by ~15% (Table 7). Each of Masarik's (2002) elemental production rates (i.e., P_{Mg}, P_{Fe}, P_{Si}, *etc.*) is then multiplied by the normalization factors to produce normalized elemental $^{3}He_c$ and $^{21}Ne_c$ production rates (i.e. J_{Mg}, J_{Fe}, J_{Si}, etc.; Table 7). Equation 3 is then used substituting J_{Mg} for P_{Mg}, etc., to calculate composition-corrected production rates based on the specific composition of an olivine. The equation below is an example for olivine (Fo_{78}):

$$\text{ex}: \frac{\left[\left(1.56 * 24.305 * J_{Mg}\right) + \left(0.44 * 55.845 * J_{Fe}\right) + \left(1 * 28.086 * J_{Si}\right) + \left(4 * 15.999 * J_{O}\right)\right]}{152.47(g/mol)} = \text{J}_{\text{M}}\ (\text{at/g/yr}) \quad . \qquad [5]$$

In this example, the resultant production rates of P_{3Hec} and P_{21Nec} in Fo_{78} are 116 and 43 at/g/yr, respectively. Similarly, composition corrected production rates can be determined for pyroxene using normalized production rates (J) for $^{3}He_c$ and $^{21}Ne_c$ and Eq. 4 to accommodate the chemical formula for pyroxene. In this study, the average composition of Bar Ten pyroxenes is En_{44} $[Ca_{0.46}Mg_{0.44}Fe_{0.10})(Si_{0.92}Al_{0.08})O_3]$.

Normalized production rates, or composition-corrected production rates, range from 117-120 and 45-47 at/g/yr for $^{3}He_c$ and $^{21}Ne_c$ in Bar Ten olivine, respectively, and are 114 and 24 at/g/yr for Bar Ten pyroxene, respectively (Table 6). Our composition-corrected production rates for $^{3}He_c$ and $^{21}Ne_c$ for Bar Ten olivine

samples (Fo_{81-84}) are equal to or higher than those in Tabernacle Hill olivine (Fo_{81}). In further agreement, composition-corrected production rates for Bar Ten pyroxenes are lower than those in Tabernacle Hill olivine (Fo_{81}). This is consistent with variations in elemental composition and specifically, with having lower production rates with lower Mg content (Schäfer et al., 1999). The production of $^{21}Ne_c$ in pyroxene predicted by our composition-correction scheme (24 at/g/yr) agrees with and is very close to our experimentally derived $P^{21}Ne_c$ (25 ± 8 at/g/yr).

Figure 10b plots the exposure ages of samples -15 (pyroxene), -16 (olivine), and -16 (pyroxene) both before compositional corrections and after. Sample -16 (olivine) changes only slightly, because the chemical composition is slightly different than that of Tabernacle Hill olivine. However, the production rate of $^{21}Ne_c$ (46 at/g/yr) appears to be too low, as the $^{21}Ne_c$ exposure age is high relative to the pyroxene samples as well as its own $^{3}He_c$ age. If a composition-corrected production rate of 50 at/g/yr is used, the $^{3}He_c$ and $^{21}Ne_c$ ages of the olivine become identical (Figure 10b). Exposure ages for both pyroxene samples (-15 and -16) calculated with $P^{21}Ne_c$ (24 at/g/yr) also have better $^{21}Ne_c$ age-agreement with sample -16 (olivine) in this case.

The ratio of production rates ($P^{21}Ne_c$ /$P^{3}He_c$) in Bar Ten samples should be equivalent to $^{21}Ne_c$ /$^{3}He_c$ values based on experimental data from this study. In Bar Ten olivine, our composition-corrected rates yield $P^{21}Ne_c$ /$P^{3}He_c$ values ranging from 0.376 to 0.392 when using $P^{3}He_c$ = 118 at/g/yr and $P^{21}Ne_c$ = 45 at/g/yr for Fo_{81} olivine, which are reasonably consistent with the average $^{21}Ne_c$/$^{3}He_c$ value of 0.400 ± 0.029, however, these ratio values are systematically lower. If we assume that $P^{3}He_c$ values of 117-120 at/g/yr are accurate for this study, we would expect $^{21}Ne_c$ to be produced in Bar Ten olivines at 47-48 at/g/yr, which is slightly higher than the 45-47 at/g/yr that are derived. Poreda and Cerling (1992) report their experimentally derived

production rate at 45 ± 4 at/g/yr, and Figure 10b shows the best 1:1 exposure age agreement in olivine (Fo_{82}) with $P^{3}He_c$ = 119 at/g/yr and $P^{21}Ne_c$ = 50 at/g/yr. If we normalize $P^{21}Ne_c$ to 49 rather than 45 at/g/yr in our composition-correction scheme, resultant production rates vary from 48-51 at/g/yr (Table 8). Most olivine data points show good agreement with the 1:1 line when ages are calculated with $^{3}He_c$ and $^{21}Ne_c$ production rates of 118 and 49 at/g/yr, and this 1:1 agreement increases with subsequent compositional corrections to these production rates (Table 8; Figure 11a and 11b).

The composition-corrected production rate of $^{21}Ne_c$ in Bar Ten clinopyroxenes is also affected by adjusting them to our normalization scheme in this manner. When normalizing $P^{21}Ne_c$ in clinopyroxenes to $P^{21}Ne_c$ = 49 at/g/yr in Fo_{81} olivine via the Masarik (2002) scheme, composition-corrected $P^{21}Ne_c$ becomes 26 at/g/yr. This increase in production rate (from 24 at/g/yr) moves Bar Ten clinopyroxene age pairs farther away from the 1:1 line by decreasing the apparent $^{21}Ne_c$ exposure age (Figure 11b). The average $^{21}Ne_c$ /$^{3}He_c$ value of 0.202 ± 0.014 in Bar Ten clinopyroxenes indicates that the production rate of $^{21}Ne_c$ in these samples should be ~23 at/g/yr, if the composition-corrected production rate of $^{3}He_c$ (114 at/g/yr) is valid and accurate. This value is closer in agreement with the $P^{21}Ne_c$ = 24 at/g/yr (composition-corrected and normalized to 45 at/g/yr) than is 26 at/g/yr. The $P^{21}Ne_c$ = 23 at/g/yr also yields the best 1:1 agreement between helium and neon ages (Figure 11c).

Given that Cerling and Craig's (1994) production rates have been verified by several independent studies and the strong age agreement shown in Figures 10 and 11, it is reasonable to conclude that the most suitable production rates of $^{21}Ne_c$ in Bar Ten olivines (Fo_{81-84}) and pyroxenes (En_{43-44}) are 48-51 at/g/yr and 23 at/g/yr, respectively (Tables 6 and 8). Exposure ages yielded by these production rates are listed in Table 8

and shown in Figures 12a and 12b for samples collected from the lower and upper Bar Ten lava flows, respectively. Excluding sample 97-AZ-330-BT, which was affected by erosion, the average (and standard deviation on) $^{3}He_{c}$ and $^{21}Ne_{c}$ ages for the lower Bar Ten flow are 99 ± 6 ka and 94 ± 4 ka, respectively, with an overall average (±standard deviation) of 96 ± 5 ka. If samples -01 and -08 are excluded on the basis that their $^{21}Ne_{c}$ and $^{3}He_{c}$ ages do not plot on the 1:1 age-relation line (Figure 11 and12) and that they may contain excess non-cosmogenic ^{3}He (as previously discussed for sample -08), both of which have the lowest $^{21}Ne_{c}$ /$^{3}He_{c}$ values (0.378 and 0.349, respectively), the average $^{3}He_{c}$ age becomes 95± 2 ka. Samples collected from the upper Bar Ten flow yield average (and standard deviation on) $^{3}He_{c}$ and $^{21}Ne_{c}$ ages of 91 ± 5 ka and 91 ± 6 ka, respectively, with an overall average (±standard deviation) of 91 ± 5 ka . These ages are bracketed by our $^{40}Ar/^{39}Ar$ ages (Figure 12a and 12b).

Though the surface exposure and $^{40}Ar/^{39}Ar$ ages of the upper and lower flows overlap within error, the petrological differences between them indicate they are separate flows with very similar eruption ages. Disagreement of ages within data sets for the upper and lower Bar Ten flows may indicate that individual sample sites were very locally and differentially affected by erosion, thus resulting in some ages that are younger than others, as previously described for samples collected in the 1997 field season (Fenton et al., 2001).

6. Conclusions

Our results emphasize the importance of using combined geochemical, petrological, and geochronological data to distinguish and age-date lava flows of very similar ages that are otherwise indistinguishable; age data alone cannot distinguish

two separate flows. The REE patterns of the two Bar Ten basalt flows differ and match the differences in petrology (i.e. the absence of pyroxene in the lower flow), indicating two separate basalt flows. Exposure ages and $^{40}Ar/^{39}Ar$ ages are nominally different and are consistent with the upper flow being younger and overlying the lower flow.

Surface exposure age-data indicate that cosmogenic ^{3}He and ^{21}Ne are extremely useful in determining eruption ages of olivine- and pyroxene-rich basaltic lava flows, particularly where obtaining accurate $^{40}Ar/^{39}Ar$ ages is problematic because of low K concentrations, high glass content, and excess Ar present in young basalts. When paired, the two isotopes offer an even stronger method of identifying non-cosmogenic components and problematic data, or outliers, within data sets containing multiple samples from one landform and/or within co-existing minerals of one rock sample. In this study, noble-gas and elemental-concentration measurements on both pyroxenes and olivines greatly increase the accuracy of $^{3}He_c$ and $^{21}Ne_c$ production rates and resulting exposure ages. When there is a discrepancy between the exposure ages, we can use the $^{21}Ne_c/^{3}He_c$ data from our samples to evaluate whether there is, for example, the presence of excess non-cosmogenic ^{3}He. Likewise, discrepancy between $^{3}He_c$ and $^{21}Ne_c$ ages can be used to evaluate the production rates published and discussed in the literature. $^{21}Ne_c/^{3}He_c$ values are 0.400 ± 0.029 and 0.202 ± 0.014 for olivine and pyroxene in this study. These values are consistent with previously published values (Poreda and Cerling, 1992; Schäfer et al., 1999; Niedermann et al., 2007) and indicate that $^{21}Ne_c/^{3}He_c$ in olivine and pyroxene remains constant with latitude, elevation, and time (up to 10 Ma). Likewise, erosion has no effect on the ratio. The neon three-isotope diagram can also indicate whether or not all excess neon in mineral separates comes from cosmogenic sources.

Experimentally calibrated production rates give more accurate surface exposure ages than those of composition-based model calculations, but the model scheme of Masarik (2002) can be used to adjust calibrated production rates for differences in major-element chemistry**.** Much attention has been paid in recent studies to correcting for effects of radiogenic and nucleogenic ^{3}He and ^{4}He to get the most accurate exposure ages. We agree this is important, however, equal attention should be paid to the effect that differences in major-element chemistry have on $^{3}He_c$ and $^{21}Ne_c$ exposure ages. Data in this study also show that $^{21}Ne_c$ production rates, and thus $^{21}Ne_c$ exposure ages, are more sensitive to changes in major-element chemistry than are $^{3}He_c$ production rates.

Based on an average $^{40}Ar/^{39}Ar$ age of 80 ± 25 ka, the production rate of $^{21}Ne_c$ in clinopyroxene is approximately 25 ± 8 at/g/yr, which is in agreement with a normalized, composition-based production rate of 24-26 at/g/yr. The production rate of $^{21}Ne_c$ as calculated from multiplying our experimentally derived $^{21}Ne_c/^{3}He_c$ value with $P^{3}He_c$ is 23 at/g/yr. This is also in agreement with our estimated $P^{21}Ne_c$ and it yields much better agreement in $^{3}He_c$ and $^{21}Ne_c$ age-pairs for all pyroxene samples in this study. The production rate of $^{21}Ne_c$ in olivine has been previously reported as 45 ± 4 at/g/yr (Poreda and Cerling, 1992), but based on our findings, it is likely to be 49 at/g/yr in Fo_{81}, when scaled with Lal's (1991) scaling factors in CosmoCalc.

In summary, data from this study indicates that the following production rates are most accurate for olivines (Fo_{81-84}) and clinopyroxenes (En_{43-44}): $P^{3}He_c$ = 117-120 and 114 at/g/yr, respectively; and $P^{21}Ne_c$ = 48-51 and 23 at/g/yr, respectively (Table 8).

Acknowledgements: We gratefully acknowledge technical and laboratory support from Enzio Schnabel, Oona Appelt, Sabine Tonn, Knut Hahne, Heike Rothe, Hartmut Liep and Marina Ospald. We especially thank Fin Stuart and Christoph Schnabel as well as other CRONUS-EU colleagues for helpful critical discussions and reviews. Two anonymous reviewers provided constructive reviews that have helped to improve this manuscript. This study was funded by the EU Marie Curie Research and Training Network "CRONUS-EU" (RTN Project Reference 511927).

References

Andrews, J.N., 1985. The isotopic composition of radiogenic helium and its use to study groundwater movement in confined aquifers, Chem. Geol. 49, 339-351.

Andrews, J.N., Kay, R.L.F., 1982. Natural production of tritium in permeable rocks. Nature 298, 361-363.

Balco, G., Shuster, D.L., 2009. Production rate of cosmogenic ^{21}Ne in quartz estimated from ^{10}Be, ^{26}Al, and ^{21}Ne concentrations in slowly eroding Antarctic bedrock surfaces. Earth Planet. Sci. Lett. 281, 48-58.

Blard, P.-H., Farley, K.A., 2008. The influence of radiogenic ^{4}He on cosmogenic ^{3}He determinations in volcanic olivine and pyroxene. Earth Planet. Sci. Lett. 276, 20–29.

Blard, P.-H., Lavé, J., Pik, R., Quidelleur, X., Bourlès, D., Kieffer, G., 2005. Fossil cosmogenic ^{3}He record from K-Ar dated basaltic flows of Mount Etna volcano (Sicily, 38º N): Evaluation of a new paleoaltimeter. Earth Planet. Sci. Lett. 236, 613-631.

Blard, P.-H., Pik, R., Lavé, J., Bourlès, D., Burnard, P.G.,Yokochi, R., Marty, B., Trusdell, F., 2006. Cosmogenic ^{3}He production rates revisited from evidences of grain size dependent release of matrix-sited helium. Earth Planet. Sci. Lett. 247, 222-234.

Blard, P.-H., Lavé, J., Pik, R., Wagnon, P., and Bourlès, D., 2007. Persistence of full glacial conditions in the Central Pacific until 15,000 years ago. Nature 449, 591-594.

Brenan, J.M., Neroda, E., Lundstrom, C.C., Shaw, H.F., Ryerson, F., Phinney, D.L., 1999. Behaviour of boron, beryllium, and lithium during melting and crystallization: Constraints from mineral-melt partitioning experiments. Geochim. Cosmochim. Acta 62, 2129-2141.

Cerling, T.E., 1990. Dating geomorphologic surfaces using cosmogenic ^{3}He. Quat. Res. 33, 148-156.

Cerling, T.E., Craig, H., 1994. Cosmogenic ^{3}He production rates from 39º N to 46º N latitude, western USA and France. Geochim. Cosmochim. Acta 58, 249-255.

Chan, L.H., Frey, F.A., 2003. Lithium isotope geochemistry of the Hawaiian plume: results from the Hawaii Scientific Drilling Project and Koolau Volcano. Geochem. Geophys. Geosyst. 4, 8707, doi: 10.1029/2002GC000365.

Craig, H., Poreda, R.J., 1986. Cosmogenic ^{3}He in terrestrial rocks: The summit lavas of Maui. Proc. Nat. Acad. of Sci. USA 83, 1970–1974.

Dunai, T.J., 2000. Scaling factors for production rates of in situ produced cosmogenic nuclides: a critical reevaluation. Earth Planet. Sci. Lett. 176, 157-169.

Dunai, T.J., Stuart, F.M., Pik, R., Burnard, P., Gayer, E., 2007. Production of ^{3}He in crustal rocks by cosmogenic thermal neutrons. Earth Planet. Sci. Lett. 258, 228-236.

Evenstar, L.A., Hartley, A.J., Stuart, F.M., Mather, A.E., Rice, C.M., Chong, G., 2009. Multiphase development of the Atacama planation surface recorded by cosmogenic ^{3}He exposure ages: Implications for uplift and Cenozoic climate change in western South America. Geology 37, 27-30. doi: 10.1130/G25437A.1.

Farley, K.A., Wolf, R.A., Silver, L.T., 1996. The effects of long alpha-stopping distances on (U-Th)/He ages. Geochim. Cosmochim. Acta 60, 4223-4229.

Fenton, C.R., Webb, R.H., Pearthree, P.A., Cerling, T.E., Poreda, R.J., 2001. Displacement rates on the Toroweap and Hurricane faults: Implications for Quaternary downcutting in Grand Canyon. Geology 29, 1035-1038.

Fenton, C.R., Webb, R.H., Cerling, T.E., Poreda, R.J., Nash, B.P., 2002. Cosmogenic ^{3}He ages and geochemical discrimination of lava-dam outburst-flood deposits in western Grand Canyon, Arizona. In House, P.K. et al. (Eds.), Ancient Floods and Modern Hazards: Principles and Applications of Paleoflood Hydrology. Amer. Geophys. Union, Water Sci. and App. Series 4, Washington, D.C., pp. 191-215.

Fenton, C.R., Poreda, R.J., Nash, B.P., Webb, R.H., Cerling, T.E., 2004. Geochemical discrimination of five Pleistocene lava-dam outburst-flood deposits, Grand Canyon. J. Geol. 112, 91-110.

Gayer, E., Mukhopadhyay, S., Meade, B.J., 2008. Spatial variability of erosion rates inferred from the frequency distribution of cosmogenic ^{3}He in olivines from Hawaiian river sediments. Earth Planet. Sci. Lett. 206, 303-315.

Gosse, J.C., Phillips, F.M., 2001. Terrestrial in situ cosmogenic nuclides: theory and application. Quat. Sci. Rev. 20, 1475-1560.

Govindaraju, K. (ed.), 1994. Compilation of working values and sample description for 383 geostandards. Geostandards Newsletter 18, Special Issue, 158 pp.

Hamblin, W.K., 1994. Late Cenozoic lava dams in the western Grand Canyon. Geol. Soc. Amer. Memoir 183, 139 p.

Holmes, R.D., Best, M.G., Hamblin, W.K., 1978. Calculated strain rates and their implications for the development of the Hurricane and Toroweap faults, Utah and northern Arizona. U.S. Geological Survey Technical Report Summaries, Earthquake Hazards Reduction Program VII, 44-50.

Imai, N., Terashima, S., Itoh, S., Ando, A., 1995. 1994 compilation of analytical data for minor and trace elements in seventeen GSJ geochemical reference samples, “Igneous Rock Series:. Geostandard News. 19, 135-213.

Kober, F., Ivy-Ochs, S., Leya, I., Baur, H., Magna, T., Wieler, R., Kubik, P.W., 2005. In situ cosmogenic ^{10}Be and ^{21}Ne in sanidine and in situ cosmogenic ^{3}He in Fe-Ti-oxide minerals. Earth Planet. Sci. Lett. 236, 404-418.

Koppers, A.A.P., Staudigel, H., Wijbrans, J.R., 2000. Dating crystalline groundmass separates of altered Cretaceous seamount basalts by the Ar-40/Ar-39 incremental heating technique. Chem. Geol. 166, 139-158.

Kounov, A., Niedermann, S., de Wit, M.J., Viola, G., Andreoli, M., Erzinger, J., 2007. Present denudation rates at selected sections of the South African escarpment and the elevated continental interior based on cosmogenic ^{3}He and ^{21}Ne. South African Journal of Geology 110, 235-248.

Kurz, M.D., 1986. Cosmogenic helium in terrestrial igneous rocks. Nature 320, 435-439.

Lal, D., 1987. Production of ^{3}He in terrestrial rocks. Chem. Geol. 66, 89-98.

Lal, D., 1991. Cosmic ray labeling of erosion surfaces: in situ nuclide production rates and erosion models. Earth Planet. Sci. Lett. 104, 424–439.

Laughlin, A.W., Poths, J., Healey, H.A., Reneau, S., WoldeGabriel, G., 1994. Dating of Quaternary basalts using the cosmogenic ^{3}He and ^{14}C methods with implications for excess ^{40}Ar. Geology 22, 135-138.

Licciardi, J.M., Kurz, M.D., Curtice, J.M., 2006. Cosmogenic ^{3}He production rates from Holocene lava flows in Iceland. Earth Planet. Sci. Lett. 246, 251-264.

Mamyrin, B.A., Tolstikhin, I.N., 1984. Helium isotopes in nature. Elsevier, Amsterdam.

Margerison, H.R., Phillips, W.M., Stuart, F.M., Sugden, D.E., 2005. Cosmogenic ^{3}He concentrations in ancient flood deposits from the Coombs Hills, northern Dry Valleys, East Antarctica: interpreting exposure ages and erosion rates. Earth Planet. Sci. Lett. 230, 163-175.

Masarik, J., 2002. Numerical simulation of in situ production of cosmogenic nuclides. Geochim. Cosmochim. Acta 66 (15A), A491.

Masarik, J., Reedy, R.C., 1996. Monte Carlo simulation of in-situ-produced cosmogenic nuclides. Radiocarbon 38, 163.

Niedermann, S., 2002. Cosmic-ray-produced noble gases in terrestrial rocks: Dating tools for surface processes. In: Noble Gases in Geochemistry and Cosmochemistry. Porcelli, D., Ballentine, C.J., Wieler, R., (Eds.), Rev. Min. Geochem. 47, 731-784.

Niedermann, S., Bach, W., Erzinger, J., 1997. Noble gas evidence for a lower mantle component in MORBs from the southern East Pacific Rise: decoupling of helium and neon isotope systematics. Geochim. Cosmochim. Acta 61, 2697–2715.

Niedermann, S., Schaefer, J.M., Wieler, R., Naumann, R., 2007. The production rate of cosmogenic ^{38}Ar from calcium in terrestrial pyroxene. Earth Planet. Sci. Lett. 257, 596-608.

Poreda, R.J, Cerling, T.E., 1992. Cosmogenic neon in recent lavas from the western United States. Geophys. Res. Lett. 19, 1863–1866.

Ryan, J.G., Kyle, P.R., 2004. Lithium abundance and lithium isotope variations in mantle sources: insights from intraplate volcanic rocks from Ross Island and Marie Byrd Land (Antarctica) and other oceanic islands. Chem. Geol. 212, 125-142.

Schäfer, J.M., Ivy-Ochs, S., Wieler, R., Leya, I., Baur, H., Denton, G.H., Schlüchter, C., 1999. Cosmogenic noble gas studies in the oldest landscape on Earth: surface exposure ages of the Dry Valleys, Antarctica. Earth Planet. Sci. Lett. 167, 215-226.

Schneider, B., Kuiper, K., Postma, O., Wijbrans, J., 2009, submitted. $^{40}Ar/^{39}Ar$ geochronology using a quadrupole mass spectrometer. Quat. Geochron. (this issue).

Seitz, H.-M., Brey, G.P., Lahaye, Y., Durali, S., Weyer, S., 2004. Lithium isotopic signatures of peridotite xenoliths and isotopic fractionation at high temperature between olivine and pyroxene. Chem. Geol. 212, 163-177.

Stone, J.O., 2000. Air pressure and cosmogenic isotope production. J. Geophys. Res. 105, 23753–23759.

Taylor, S.R., McClennan, S.M., 1985. The Continental Crust: its composition and evolution. Blackwell Sci. Pub., London, 312 pp.

Vermeesch, P., 2007. CosmoCalc: An Excel add-in for cosmogenic nuclide calculations. Geochem. Geophys. Geosyst. 8, Q08003, doi: 10.1029/2006GC001530.

Wells, S.G., McFadden, L.D., Poths, J., Olinger, C.T., 1995. Cosmogenic ^{3}He surface-exposure dating of stone pavements: Implications for landscape evolution in deserts. Geology 23, 613-616.

Ziegler, J.F., 1977. Helium: Stopping powers and ranges in all elemental matter. Pergamon.

Figure 1. Location of the Bar Ten lava flows, two Pleistocene basalt flows that erupted very closely in time in the Uinkaret volcanic field in western Grand Canyon National Park, Arizona, USA. Dark gray areas represent cinder cones and light gray areas represent lava flows. Arrows point out general locations of the upper and lower Bar Ten flows.

Figure 2. Chondrite-normalized REE patterns and related La/Sm and Gd/Lu ratios of whole-rock basalts collected from the upper (051210-04) and lower (051110-03) Bar Ten basalt flows.

Figure 3. Digital orthophotograph (a) of the Bar Ten lava mass with sample locations on the upper and lower flows for surface exposure dating. The individual flows are not mapped because contacts are not distinguishable in the field or in aerial photographs with any certainty. See text for details. Full white circles indicate samples collected during the 2005-2006 field season. Circles with black dots (labeled E, F, and G) indicate samples that were collected in 1997. The vertical profile (b) is constructed from the line Z-Z' in (a) and elevations of sample locations are projected onto this line. Two straight dashed lines point out a major strand of the normal Hurricane Fault that crosscuts the Bar Ten flow, and has up to 10 ± 3 m of offset (Fenton et al., 2001).

Figure 4. (a) Photograph of the top of a pressure ridge near where samples 240406-06, -08, and -09 were collected. View is to the south. (b) Resistant, smooth surface of a massive pressure ridge. Samples 051110-01, -03, 240406-06, -08, and -09 were collected from surfaces like this one.

Figure 5. Photograph of pahoehoe structures typical to those found on the Bar Ten lava flow. Sample 240406-10 was collected from the ropy surface in this photo.

Figure 6. Concentrations of (a) $^{3}He_{c}$ and (b) $^{21}Ne_{c}$ in olivine and pyroxene mineral separates from basalt samples as a function of elevation. The solid ellipses in (a) and (b) point out agreement in $^{3}He_{c}$ concentrations in samples 250406-15 and -16 (olivine and pyroxene) and $^{21}Ne_{c}$ in samples -15 and -16 pyroxene from the same sample site. The dashed ellipses indicate samples collected in 1997 and analyzed for $^{3}He_{c}$ at the University of Rochester in a previous study (Fenton et al., 2001). One replicate sample (97-AZ-330-BT) from this group was analyzed again for $^{3}He_{c}$ and $^{21}Ne_{c}$ at the GFZ Potsdam in 2007 (see text).

Figure 7. Five samples (3 olivine, 2 pyroxene) that were crushed in vacuo plotted in a neon three-isotope diagram. Step-wise heating data plotting close to atmosphere are also shown. See Figure 8 for all step-wise heating data.

Figure 8. Neon three-isotope diagram showing data from (a) olivines and (b) pyroxenes measured at two or three temperature steps (600º, 900º, and 1750º C). An error-weighted regression defines a spallation line [$y = (1.033 \pm 0.031)x + (0.09876 \pm 0.00033)$] through our olivine data, which is, within uncertainties, indistinguishable from the line for pyroxene shown in (b) (Schäfer et al., 1999). Small dashed lines represent the error bands of the olivine and pyroxene spallation lines. Notice that all data fall on the spallation lines.

Figure 9. $^{21}Ne_c/^{3}He_c$ ratios in olivine and pyroxene separates from basalt samples as a function of elevation.

Figure 10. (a) Graph illustrating $^{3}He_c$ and $^{21}Ne_c$ ages calculated using experimentally determined and compositional-based calculated production rates for samples 250406-15 (pyroxene), -16 (pyroxene) and -16 (olivine). High latitude, sea-level rates used for calculating data in the Calibrated group are based on Poreda and Cerling (1992), Cerling and Craig (1994), and this study and are as follows: $P^{3}He_c$ (olivine/pyroxene) = 118 at/g/yr; $P^{21}Ne_c$ (olivine) = 45 at/g/yr; $P^{21}Ne_c$ (pyroxene) = 25 at/g/yr. Rates used in the Masarik and Kober groups are based on model calculations from Masarik (2002) and Kober et al. (2005) and are listed in Table 6. All production rates are scaled identically for each sample with CosmoCalc (Vermeesch, 2007) using Lal (1991). (b) Graph illustrating ages of samples 250406-15 and -16 after correcting data in the Calibrated group with Masarik (2002) for elemental chemistry. The gray square represents exposure ages yielded by sample -16 (olivine) when $P^{3}He_c$ = 119 at/g/yr and $P^{21}Ne_c$ = 50 at/g/yr. See text for details. Error bars do not include production rate uncertainties. Arrows indicate change in ages with composition and ratio corrections.

Figure 11. Ages calculated from composition-corrected $^{3}He_c$ production rates – normalized to 118 and 49 at/g/yr for Fo_{81} olivine– for Bar Ten (a) olivine and (b) pyroxene; $P^{3}He_c$ (olivine/pyroxene) = 117-120 at/g/yr; $P^{21}Ne_c$ (olivine) = 48-51 at/g/yr; $P^{21}Ne_c$ (pyroxene) = 26 at/g/yr. (c) Ages of pyroxenes calculated using $P^{21}Ne_c$ (pyroxene) = 23 at/g/yr, which is determined by multiplying $P^{3}He_c$ = 119 at/g/yr by $P^{21}Ne_c$ / $P^{3}He_c$ = 0.202. Using this $^{21}Ne_c$ production rate gives the best 1:1 age agreement in pyroxene. Arrows indicate change in ages with composition and ratio corrections.

Figure 12. Exposure ages of the (a) lower and (b) upper Bar Ten lava flows. Sample 97-AZ-330-BT was affected by erosion (see text). $^{40}Ar/^{39}Ar$ ages of the upper and lower Bar Ten flow are plotted with error bars on the 1:1 line. $^{40}Ar/^{39}Ar$ ages bracket our composition-corrected surface exposure ages. Error bars do not include production rate uncertainties.

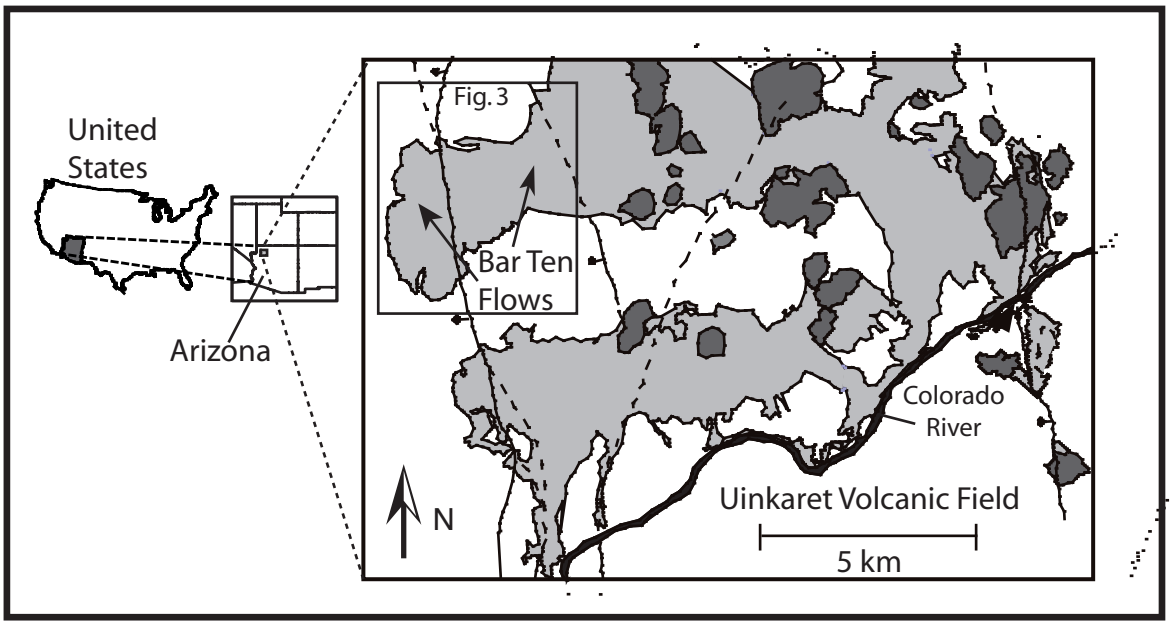
United
States
Arizona
Fig. 3
Bar Ten
Flows
Colorado
River
N
Uinkaret Volcanic Field
5 km

Figure 1.

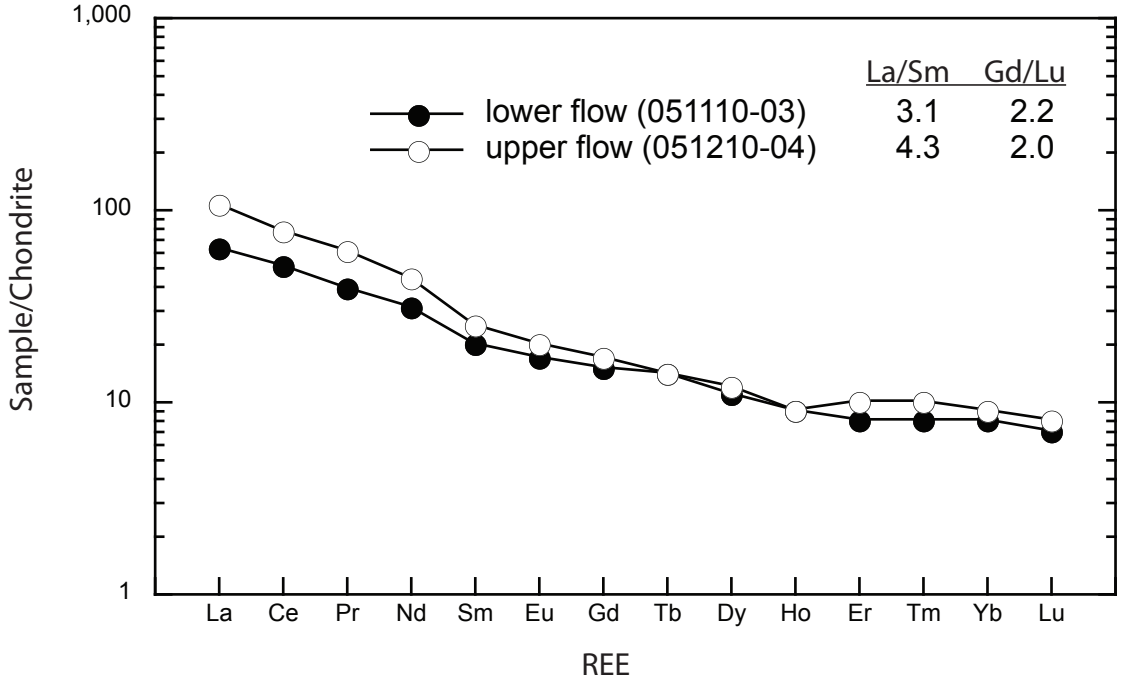
1,000
100
10
1
Sample/Chondrite
La/Sm Gd/Lu
lower flow (051110-03) 3.1 2.2
upper flow (051210-04) 4.3 2.0
La Ce Pr Nd Sm Eu Gd Tb Dy Ho Er Tm Yb Lu
REE

[Figure 2]

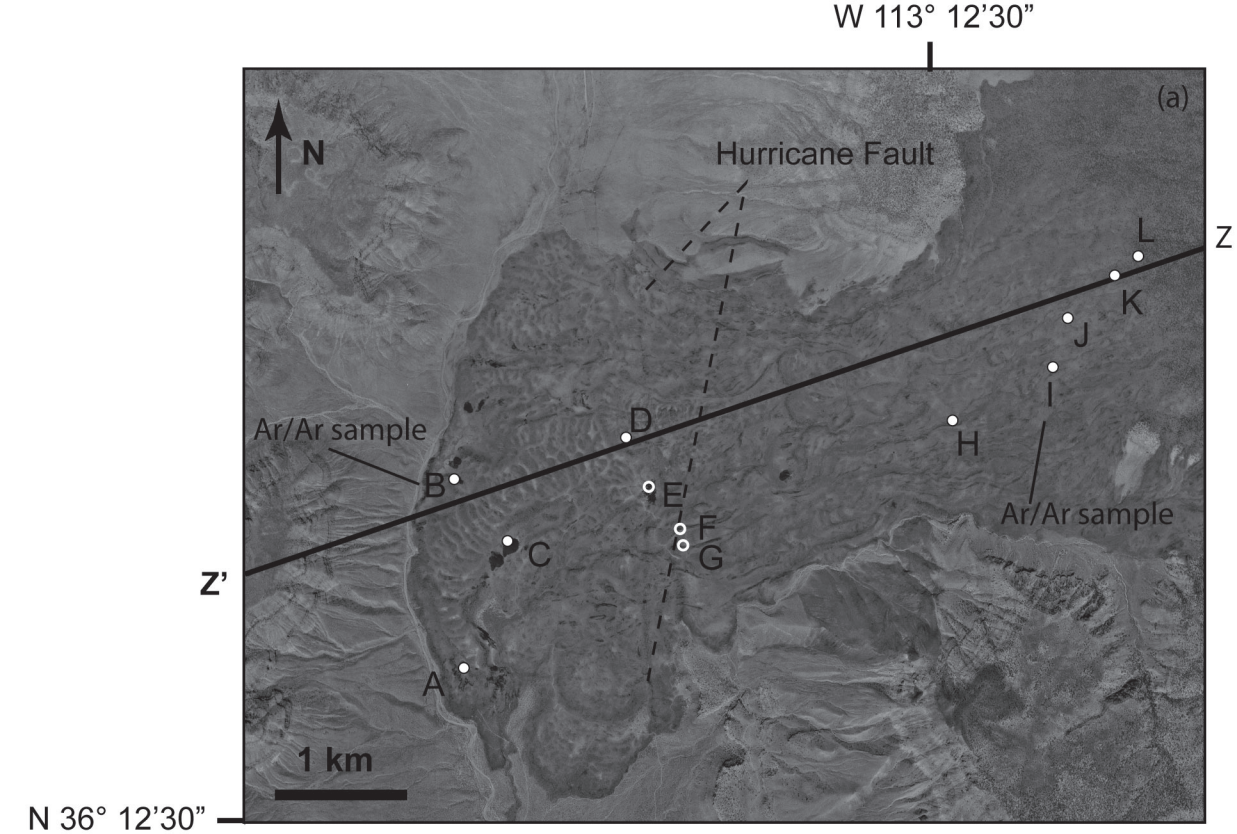

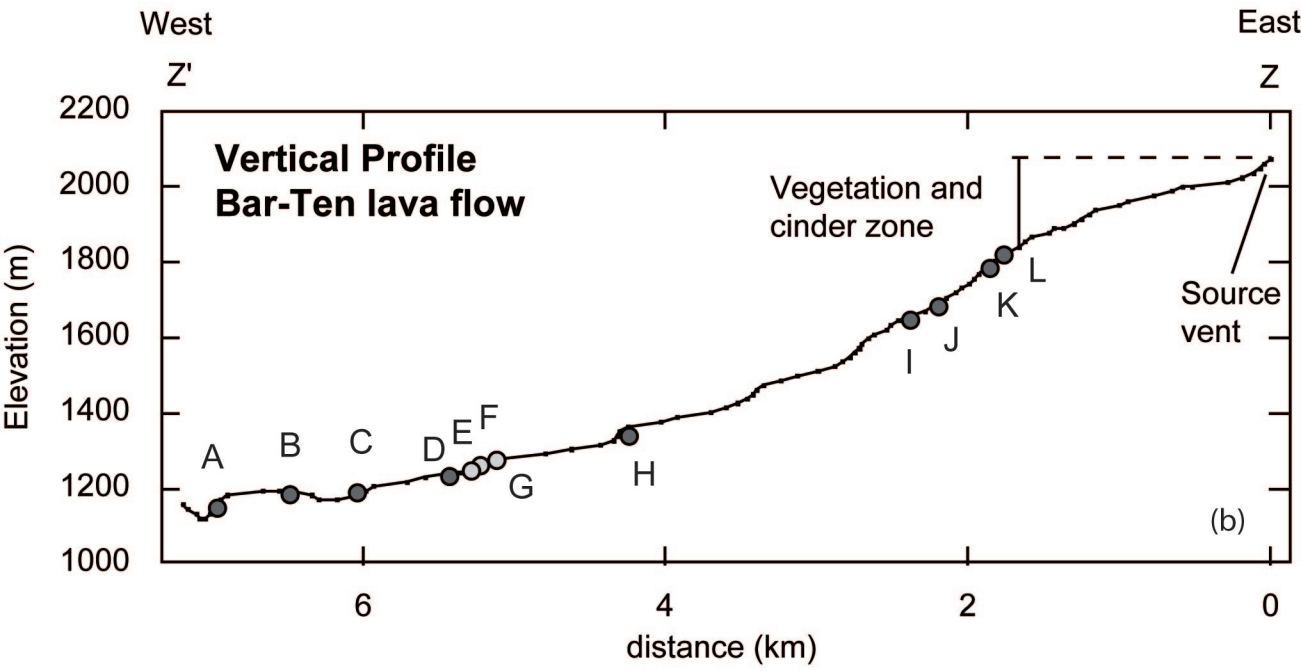

Sample Numbers and Locations

Lower flow	Upper flow
A. 240406-10 B. 051110-01, -02, and -03 C. 240406-06,-08, and-09 D. 240406-11 E. 97AZ-326, 327, 328 BT F. 97AZ330BT G. 97AZ331BT H. 260406-20	I. 051210-04, -05 J. 250406-17 K. 250406-15 and-16 L. 250406-13

Figure 3.

Figure 4

Figure 5

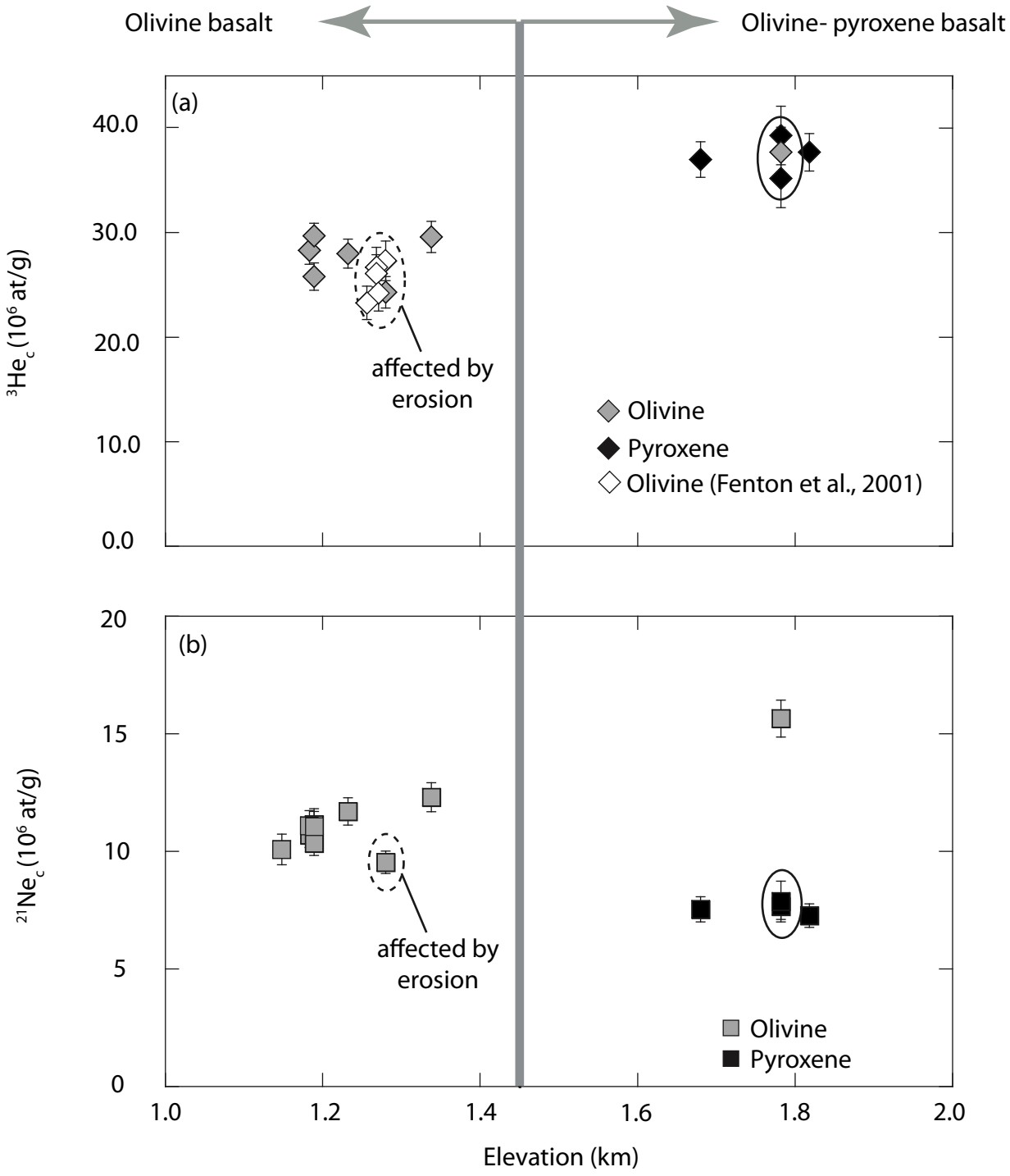
Olivine basalt
Olivine- pyroxene basalt
(a)
40.0
30.0
20.0
10.0
0.0
^3He_c (10^6 at/g)
affected by erosion
Olivine
Pyroxene
Olivine (Fenton et al., 2001)
(b)
20
15
10
5
0
$^{21}Ne_c$ (10^6 at/g)
affected by erosion
Olivine
Pyroxene
1.0
1.2
1.4
1.6
1.8
2.0
Elevation (km)

[Figure 6]

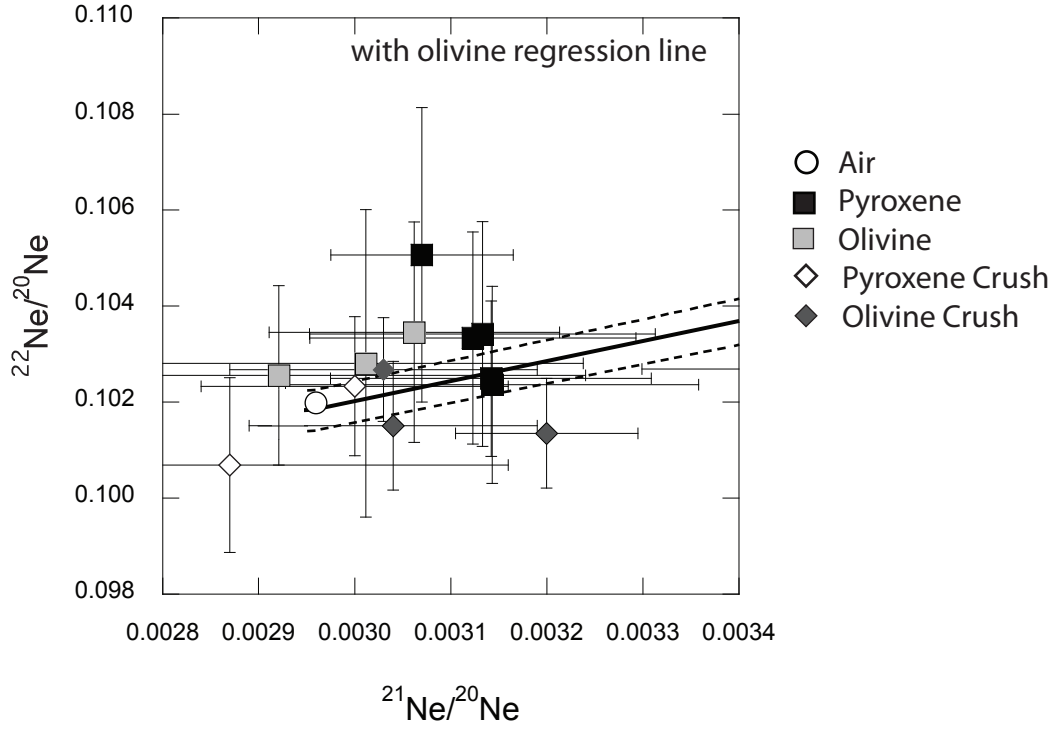
with olivine regression line
0.110
0.108
0.106
0.104
0.102
0.100
0.098
0.0028
0.0029
0.0030
0.0031
0.0032
0.0033
0.0034
$^{22}Ne/^{20}Ne$
$^{21}Ne/^{20}Ne$
Air
Pyroxene
Olivine
Pyroxene Crush
Olivine Crush

[Figure 7]

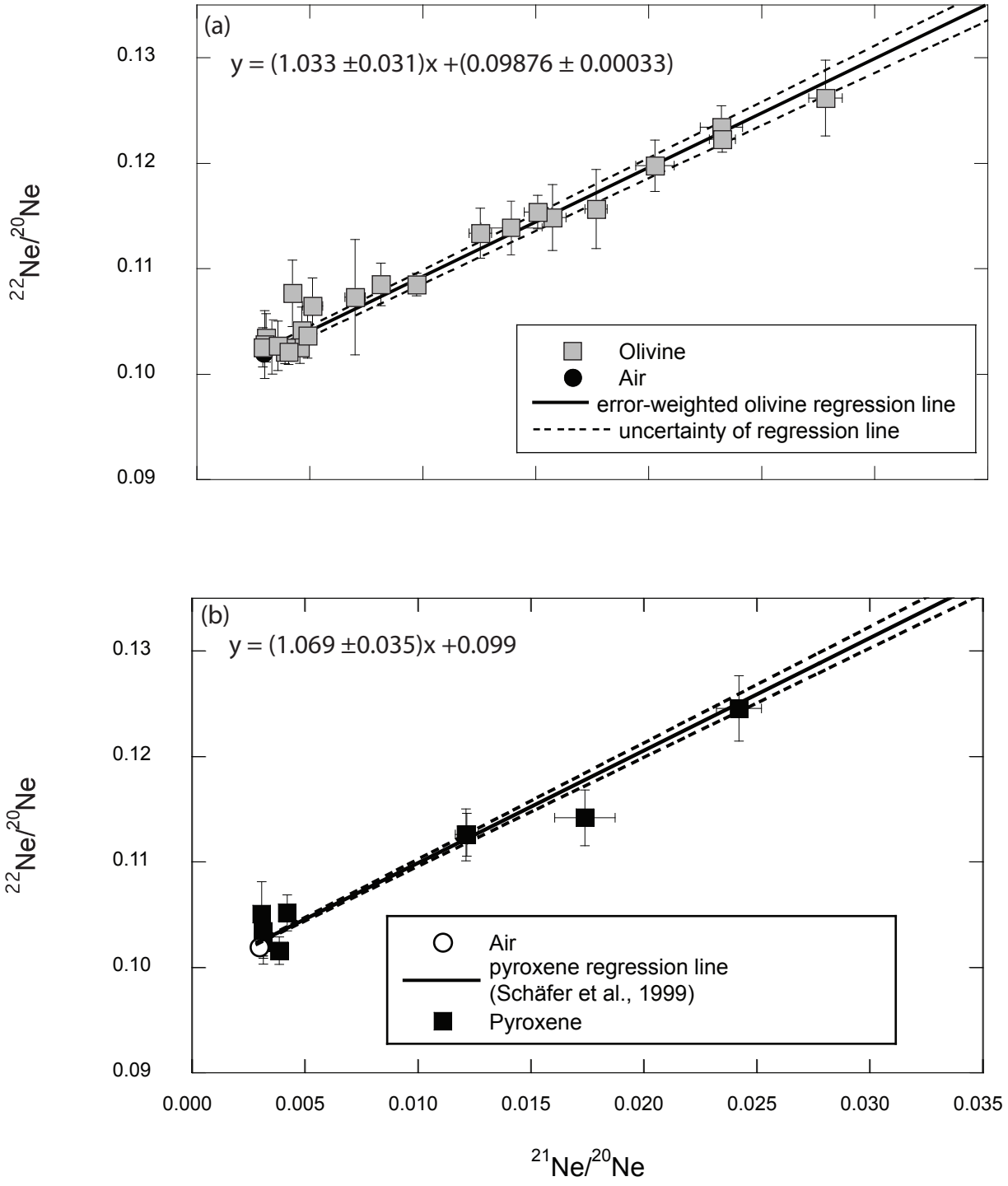
(a)
y = (1.033 ±0.031)x +(0.09876 ± 0.00033)
0.13
0.12
0.11
0.10
0.09
22Ne/20Ne
Olivine
Air
error-weighted olivine regression line
uncertainty of regression line
(b)
y = (1.069 ±0.035)x +0.099
0.13
0.12
0.11
0.10
0.09
22Ne/20Ne
Air
pyroxene regression line
(Schäfer et al., 1999)
Pyroxene
0.000
0.005
0.010
0.015
0.020
0.025
0.030
0.035
21Ne/20Ne

[Figure 8]

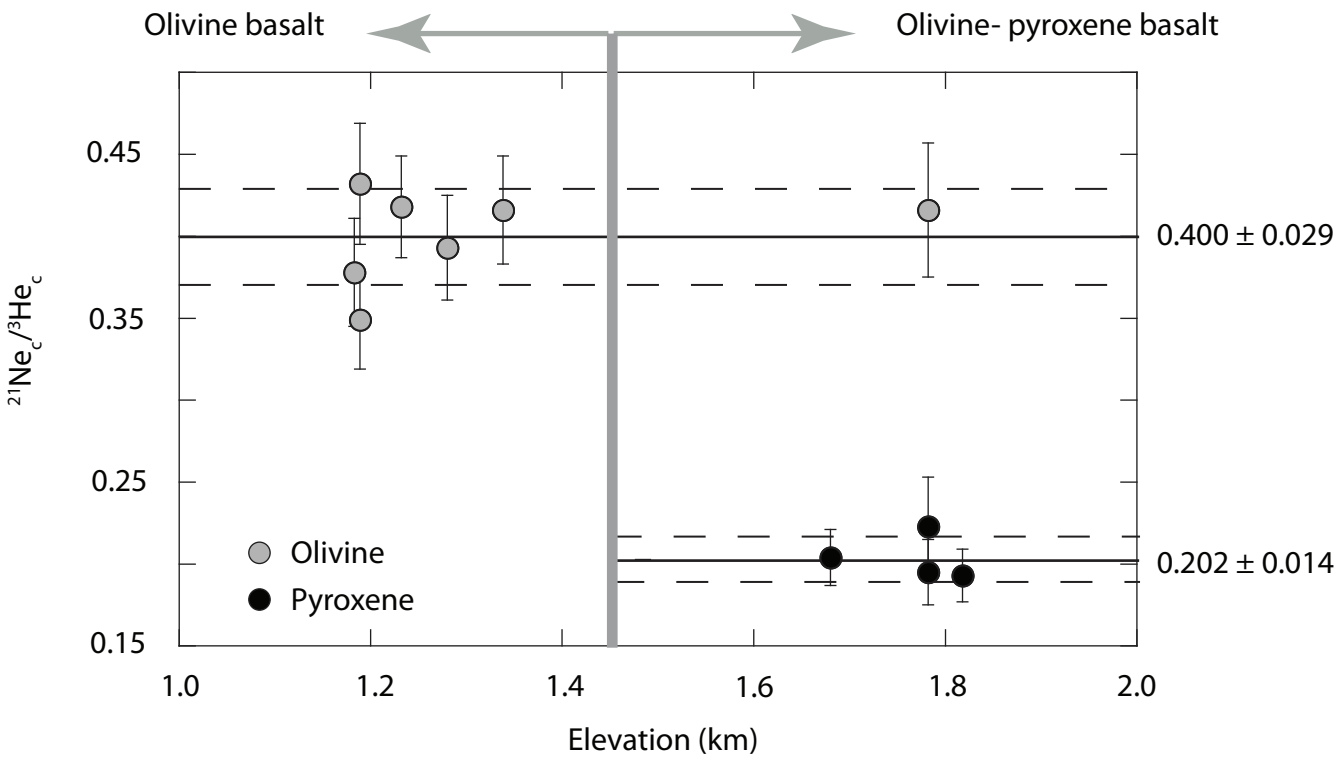
Olivine basalt
Olivine- pyroxene basalt
0.45
0.35
0.25
0.15
$^{21}Ne_c/^3He_c$
0.400 ± 0.029
0.202 ± 0.014
Olivine
Pyroxene
1.0
1.2
1.4
1.6
1.8
2.0
Elevation (km)

[Figure 9]

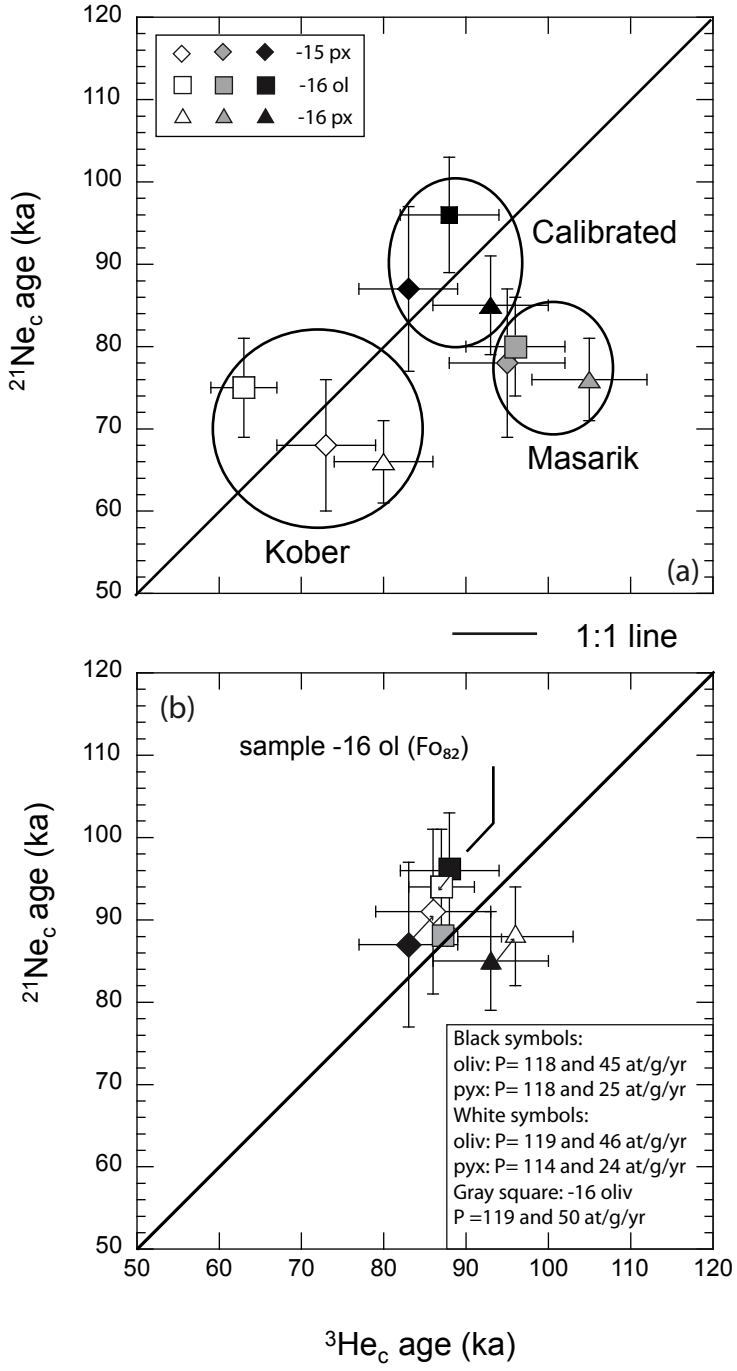
-15 px
-16 ol
-16 px
Calibrated
Masarik
Kober
(a)
1:1 line
(b)
sample -16 ol (Fo82)
Black symbols:
oliv: P= 118 and 45 at/g/yr
pyx: P= 118 and 25 at/g/yr
White symbols:
oliv: P= 119 and 46 at/g/yr
pyx: P= 114 and 24 at/g/yr
Gray square: -16 oliv
P =119 and 50 at/g/yr
21Nec age (ka)
3Hec age (ka)
50
60
70
80
90
100
110
120

[Figure 10]

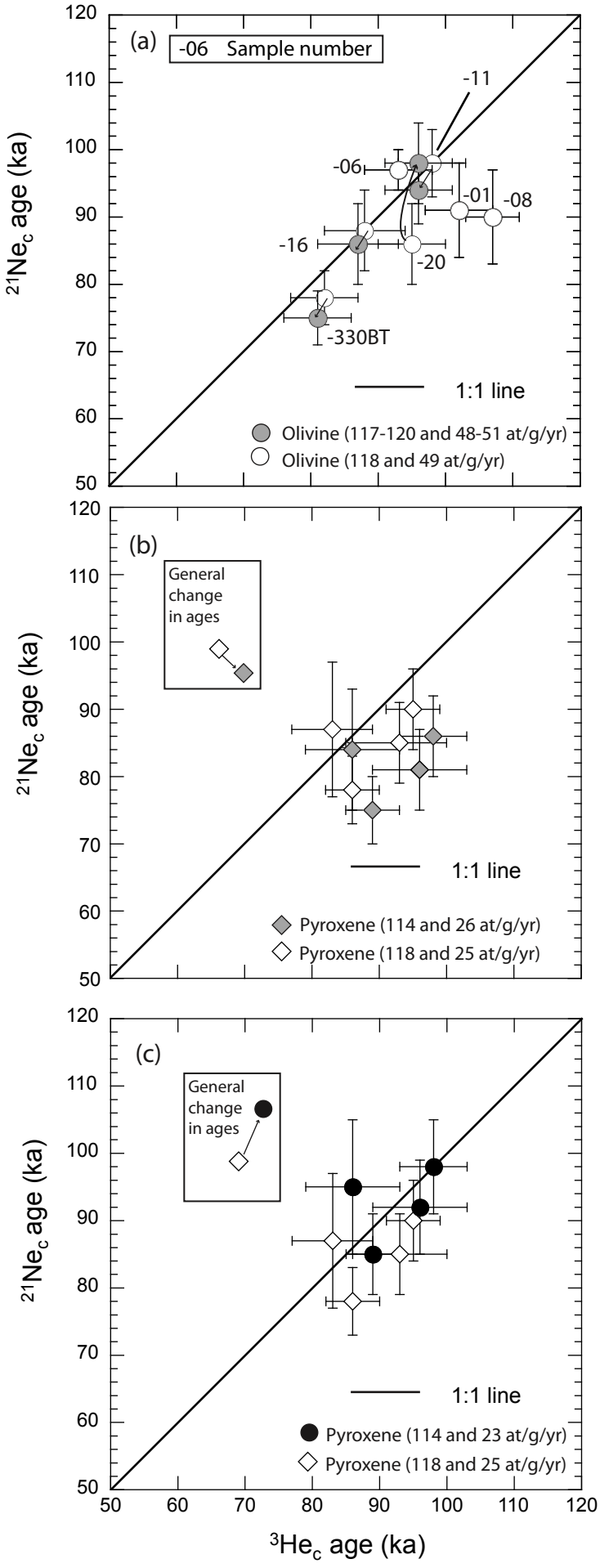
(a)
-06 Sample number
-11
-06
-01
-08
-16
-20
-330BT
1:1 line
Olivine (117-120 and 48-51 at/g/yr)
Olivine (118 and 49 at/g/yr)
(b)
General change in ages
1:1 line
Pyroxene (114 and 26 at/g/yr)
Pyroxene (118 and 25 at/g/yr)
(c)
General change in ages
1:1 line
Pyroxene (114 and 23 at/g/yr)
Pyroxene (118 and 25 at/g/yr)
$^{21}Ne_c$ age (ka)
$^{3}He_c$ age (ka)
50
60
70
80
90
100
110
120

[Figure 11]

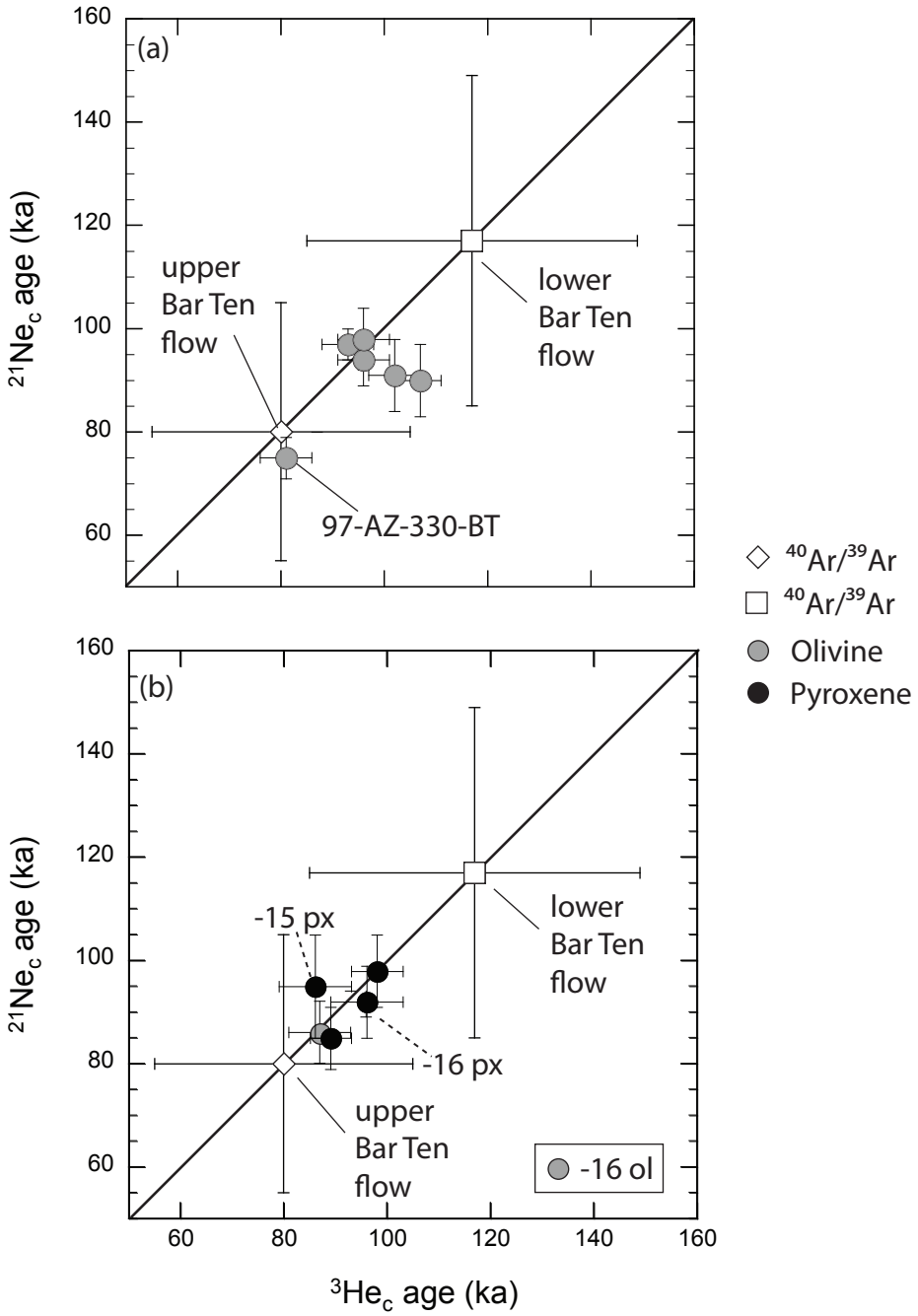
(a)
upper
Bar Ten
flow
lower
Bar Ten
flow
97-AZ-330-BT
(b)
-15 px
-16 px
lower
Bar Ten
flow
upper
Bar Ten
flow
-16 ol
$^{21}Ne_c$ age (ka)
$^{3}He_c$ age (ka)
60
80
100
120
140
160
$^{40}Ar/^{39}Ar$
$^{40}Ar/^{39}Ar$
Olivine
Pyroxene

[Figure 12]

Table 1. Information on sampling locations, sample types, and measured $^{3}He_{c}$ and $^{21}Ne_{c}$ concentrations in olivine and pyroxene separates obtained from the Bar Ten basalt flow in the Uinkaret volcanic field in western Grand Canyon, Arizona. Concentrations of $^{3}He_{c}$ and $^{21}Ne_{c}$ are calculated here using Equations 1 and 2 (see text).

Location/Sample	Locale in Figure 2a	Latitude (°N)	Longitude (°W)	Elevation (km)	Phase[a]	Size Fraction analyzed (μm)[b]	Sample thickness (cm)	Total Shielding Factor[c]	CosmoCalc Lal (1991) Scaling Factor	Cerling's Fit to Lal (1991) Scaling Factor	Sample Type	$^{3}He_{c}$[d,e] (10^{6} atoms/g)	$^{21}Ne_{c}$[d,e] (10^{6} atoms/g)	$^{21}Ne_{c}/^{3}He_{c}$[f]
Lower Bar Ten flow														
240406-10	A	36.2167	113.2384	1.148	ol	125-250	4	0.963	2.28	2.32	Pahoehoe/tumulus	--[g]	10.08±0.65	--[g]
051110-01	B	36.2279	113.2391	1.183	ol	250-500	4	0.963	2.34	2.39	Pressure ridge	28.3±1.3	10.70±0.82	0.378±0.033
051110-02	B	36.2279	113.2391	1.183	Ar/Ar	--	--	--	--	--	Pressure ridge	--	--	--
051110-03	B	36.2279	113.2391	1.183	ol	250-500	4	0.963	2.34	2.39	Pressure ridge	--[g]	11.09±0.64	--[g]
240406-06	C	36.2244	113.2357	1.189	ol	250-500	4	0.964	2.35	2.40	Pressure ridge	25.8±1.3	11.15±0.76	0.432±0.037
240406-08	C	36.2244	113.2357	1.189	ol	250-500	4	0.964	2.35	2.40	Pressure ridge	29.7±1.2	10.35±0.77	0.349±0.030
240406-09	C	36.2244	113.2357	1.189	ol	250-500	4	0.964	2.35	2.40	Pressure ridge	--[g]	11.11±0.71	--[g]
240406-11	D	36.2314	113.2268	1.232	ol	250-500	4	0.964	2.43	2.48	Pressure ridge	28.0±1.4	11.70±0.63	0.418±0.031
97-AZ-328-BT[h]	E	36.2273	113.2249	1.256	ol	250-500	4	0.964	2.47	2.52	Pahoehoe/tumulus	23.7±1.7	--	--
97-AZ-326-YBT[h]	E	36.2267	113.2249	1.268	ol	250-500	4	0.964	2.49	2.54	Pahoehoe/tumulus	27.1±1.9	--	--
97-AZ-327-YBT[h]	E	36.2270	113.2263	1.268	ol	250-500	4	0.964	2.49	2.54	Pahoehoe/tumulus	26.6±1.9	--	--
97-AZ-330-BT	F	36.2252	113.2228	1.271	ol	250-500	4	0.964	2.50	2.55	Pahoehoe/tumulus	24.3±1.5	9.54±0.51	0.393±0.032
97-AZ-330-BT[h]	F	36.2252	113.2228	1.271	ol	250-500	4	0.964	2.50	2.55	Pahoehoe/tumulus	24.5±1.7	--	--
97-AZ-331-BT[h]	G	36.2239	113.2223	1.280	ol	250-500	4	0.964	2.52	2.57	Pahoehoe/tumulus	27.3±1.9	--	--

260406-20	H	36.2307	113.2145	1.338	ol	250-500	4	0.964	2.63	2.68	Pressure ridge	29.6±1.5	12.32±0.76	0.416±0.033
Upper Bar Ten flow														
051210-05	I	36.2357	113.1949	1.646	Ar/Ar	--	--	--	--	--	Pahoehoe/tumulus	--	--	--
250406-17	J	36.2382	113.1938	1.680	px	125-250	6	0.947	3.36	3.44	Pahoehoe/tumulus	37.0±1.7	7.54±0.54	0.204±0.017
250406-15	K	36.2408	113.1904	1.782	px	125-500	4	0.964	3.62	3.70	Pahoehoe/tumulus	35.2±2.8	7.87±0.87	0.223±0.030
250406-16	K	36.2408	113.1904	1.782	ol	125-500	6	0.947	3.62	3.70	Pahoehoe/tumulus	37.7±2.4	15.7±1.2	0.416±0.041
250406-16	K	36.2408	113.1904	1.782	px	125-500	6	0.947	3.62	3.70	Pahoehoe/tumulus	39.3±2.8	7.66±0.55	0.195±0.020
250406-13	L	36.2417	113.1889	1.818	px	125-250	6	0.948	3.71	3.80	Pahoehoe/tumulus	37.7±1.8	7.27±0.50	0.193±0.016

Note: '--' indicates no available data.

[a] ol = olivine, px = pyroxene, Ar/Ar = a sample for $^{40}Ar/^{39}Ar$ dating.

[b] This size refers to the range of grain sizes resulting from the crushing/sieving of whole-rock basalt samples. Phenocrysts could have been larger in the whole-rock samples. In addition, the mineral separates were not powdered, except for sample 250406-17 px, prior to loading in the furnace.

[c] The total shielding factor includes corrections for sample depth (self-shielding) and topographic shielding; (total shielding factor = 1.0 equates to no shielding correction).

[d] Analytical uncertainty (95% confidence level) includes precision of mass spectrometer sensitivity and corrections for blanks, mass discrimination and isobaric interferences.

[e] $^{3}He_c$ and $^{21}Ne_c$ atom concentrations are corrected to the surface of each sample (self–shielding) and for topographic shielding using the total shielding factor.

[f] Uncertainty includes the analytical errors reported for $^{3}He_c$ and $^{21}Ne_c$ atom concentrations.

[g] Technical difficulties were experienced during He analyses.

[h] Analyses performed at the University of Rochester and originally reported in Fenton et al. (2001) were corrected with a crush value of $^{3}He/^{4}He = 7.22\ R_a$. $^{3}He_c$ values reported here are corrected with a crush value of $6.06\ R_a$. No neon analyses were performed on this aliquot. Samples collected from the lower Bar Ten flow in 1997 yielded concentrations of $^{3}He_c$ in olivine that range from 23.7±1.2 to 27.3±1.4 Mat/g (Mat = million atoms; reported as such in Fenton et al., 2001), when corrected with the average $^{3}He/^{4}He$ crush value of $7.22\ R_a$ for trapped gases.

Table 2. Elemental concentrations [wt. %] in Bar Ten olivine and pyroxene, based on electron microprobe and ICP-AES analyses.

Sample Number **OLIVINE**		Na[a]	Mg[a]	Al[a]	Si[a, b]	Ca[a]	Ti[a]	Cr[a]	Mn[a]	Fe[a]	Ni[a]
051110-01	**MP**	--	26.04	0.02	18.55	0.14	0.01	0.03	0.15	11.84	0.19
	ICPAES	0.06	25.92	0.24	18.28	0.35	0.04	--	--	13.06	--
051110-03	**MP**	--	25.78	0.02	18.45	0.13	0.01	0.03	0.15	12.31	0.19
	ICPAES	0.02	26.34	0.15	17.80	0.24	0.01	--	--	13.65	--
240406-06	**MP**	--	25.68	0.01	18.45	0.14	0.01	0.02	0.15	12.46	0.19
	ICPAES	0.03	31.07	0.18	13.39	0.24	0.02	--	--	14.82	--
240406-08	**MP**	--	25.70	0.02	18.43	0.13	0.01	0.03	0.16	12.43	0.19
	ICPAES	0.02	26.80	0.16	18.05	0.17	0.02	--	--	12.69	--
240406-09	**MP**	--	25.80	0.02	18.44	0.13	0.01	0.03	0.17	12.29	0.20
	ICPAES	0.02	26.27	0.14	18.69	0.22	0.02	--	--	12.29	--
240406-10	**MP**	--	23.98	0.02	18.06	0.16	0.01	0.01	0.18	15.07	0.15
	ICPAES	0.03	25.65	0.11	18.23	0.20	0.02	--	--	13.93	--
240406-11	**MP**	--	26.75	0.02	18.60	0.14	0.01	0.03	0.13	10.94	0.18
	ICPAES	0.04	27.26	0.22	18.32	0.24	0.03	--	--	11.48	--
250406-16	**MP**	--	25.96	0.02	18.56	0.16	0.01	0.02	0.14	11.97	0.14
	ICPAES	0.04	27.39	0.23	18.11	0.25	0.03	--	--	11.59	--
260406-20	**MP**	--	25.16	0.02	18.42	0.17	0.01	0.02	0.17	13.12	0.13
	ICPAES	0.02	26.91	0.06	18.91	0.14	0.02	--	--	11.31	--
97 AZ 330 BT	**MP**	--	26.97	0.02	18.80	0.13	0.01	0.03	0.11	10.39	0.19
	ICPAES	0.02	26.10	0.06	19.89	0.15	0.02	--	--	10.74	--
Sample Number **PYROXENE**											
250406-13	**MP**	0.21	9.16	1.84	24.05	15.97	0.53	0.30	0.07	4.18	0.02
	ICPAES	0.33	9.25	2.30	24.27	14.87	0.60	--	--	4.67	--
250406-15	**MP**	0.23	8.90	2.26	23.67	16.12	0.60	0.36	0.08	4.19	0.02
	ICPAES	0.19	11.28	1.68	24.24	13.21	0.46	--	--	5.18	--
250406-16	**MP**	0.19	9.33	1.68	24.19	15.97	0.49	0.26	0.09	4.09	0.01
	ICPAES	0.19	10.03	1.81	23.60	16.03	0.54	--	--	4.57	--
250406-17	**MP**	0.20	9.21	1.80	24.14	16.06	0.50	0.27	0.08	4.05	0.01
	ICPAES	0.27	11.18	2.05	23.21	13.81	0.54	--	--	5.65	--

Note: '- -' indicates data not available. MP = Electron Microprobe

[a] Total wt. % of measured elements. Silicon was not measured by ICP-AES. Oxygen was not measured by electron microprobe or ICP-AES.

[b] Weight percent silicon for ICP-AES measurements was estimated by calculating all measured elements as oxides (wt. %), subtracting this total from 100% (leaving SiO_2 wt.%), and determining the weight percent of Si in SiO_2.

Table 3. He and Ne concentrations and isotopic compositions of Bar Ten olivine and pyroxene as measured on the GFZ Potsdam noble-gas mass spectrometers by step-wise heating and crushing procedures. Data have been corrected for analytical blanks, isobaric interferences, and mass discrimination effects. Error limits correspond to 95% confidence level.

Sample	Temperature (°C)	File Name	^{4}He (10^{-8} cm^3/g)	^{20}Ne (10^{-12} cm^3/g)	$^{3}He/^{4}He$ (10^{-6})	$^{22}Ne/^{20}Ne$ (10^{-2})	$^{21}Ne/^{20}Ne$ (10^{-2})
051110-01	600	0401A	0.0933±0.0047	29.6±1.6	168±13	10.35±0.24	0.307±0.016
Olivine	900	0401B	0.0537±0.0029	9.02 ±0.65	1185±29	10.80±0.62	0.753±0.054
0.84926 g	1750	0401C	0.228±0.012	62.6±3.5	111.6±6.0	10.88±0.21	0.838±0.036
Total			0.375±0.013	101.2±3.9	279±11	10.72±0.16	0.675±0.025
051110-03							
Olivine	900	0434A	0.0779±0.0040	27.9±1.6	--[a]	10.26±0.16	0.436±0.022
0.99452 g	1750	0434B	0.1652±0.0085	23.0±1.3	--[a]	11.62±0.39	1.825±0.055
Total			0.2431±0.0094	50.9±2.1	--	10.87±0.20	1.064±0.039
240406-06							
Olivine	900	P183A	0.1556±0.0079	29.9±1.6	408±13	10.21±0.12	0.394±0.021
0.99602 g	1750	P183B	0.390±0.020	29.1±1.6	86.5±6.3	11.61±0.17	1.572±0.066
Total			0.546±0.022	59.0±2.3	178.2±7.5	10.90±0.11	0.975±0.041
240406-08	600	0402A	0.0487±0.0030	25.6±1.4	150±13	10.26±0.19	0.292±0.033
Olivine	900	0402B	0.0648±0.0034	19.7±1.1	978±20	10.80±0.33	0.429±0.029
0.96324 g	1750	0402C	0.407±0.021	34.7±2.0	98.9±2.9	11.38±0.25	1.295±0.054
Total			0.521±0.021	80.0±2.7	213.1±7.7	10.88±0.15	0.761±0.031
240406-09							
Olivine	900	0432A	0.1373±0.0070	23.1±1.4	--[a]	10.43±0.23	0.473±0.012
0.99982 g	1750	0432B	0.408±0.021	16.58±0.98	--[a]	12.48±0.22	2.46±0.11
Total			0.545±0.022	39.7±1.7	--	11.29±0.17	1.303±0.062
240406-10							
Olivine	900	0433A	0.197±0.010	25.3±1.5	--[a]	10.38±0.22	0.500±0.028
0.99156 g	1750	0433B	0.0713±0.0039	23.3±1.3	--[a]	11.54±0.33	1.623±0.066
Total			0.268±0.011	48.6±2.0	--	10.94±0.20	1.038±0.042
240406-11							
Olivine	900	P184A	0.258±0.013	39.1±2.1	289.2±8.0	10.251±0.085	0.3962±0.0089
1.65458 g	1750	P184B	1.194±0.060	17.8±1.0	31.9±1.8	12.33±0.13	2.429±0.067
Total			1.452±0.061	56.9±2.3	77.6±3.4	10.901±0.079	1.032±0.040

Sample	Temperature (°C)	File Name	^{4}He (10^{-8} cm^3/g)	^{20}Ne (10^{-12} cm^3/g)	$^{3}He/^{4}He$ (10^{-6})	$^{22}Ne/^{20}Ne$ (10^{-2})	$^{21}Ne/^{20}Ne$ (10^{-2})
250406-16							
Olivine	900	P182A	0.246±0.013	49.9±3.2	387±20	10.28±0.26	0.364±0.031
0.25012 g	1750	P182B	0.646±0.037	23.9±2.3	69.6±6.4	12.42±0.34	2.46±0.18
Total			0.892±0.039	73.8±3.9	157.4±8.7	10.97±0.21	1.043±0.082
260406-20	600	0415A	0.226±0.011	19.6±1.2	12.7±1.3	10.29±0.34	0.302±0.024
Olivine	900	0415B	1.819±0.091	15.71±0.97	52.3±1.3	10.68±0.28	0.528±0.048
1.00156 g	1750	0415C	1.224±0.062	14.5±1.0	29.2±1.5	12.92±0.42	3.09±0.13
Total			3.27±0.11	49.8±1.8	40.9±1.0	11.18±0.21	1.185±0.062
97-AZ-330-BT							
Olivine	900	P173A	0.1416±0.0071	20.4±1.1	311±21	10.21±0.13	0.410±0.019
1.20346 g	1750	P173B	1.367±0.069	46.2±2.4	40.8±2.3	10.86±0.11	0.987±0.016
Total			1.509±0.069	66.6±2.6	66.2±3.3	10.66±0.09	0.810±0.016
250406-13	600	0413A	0.0905±0.0048	36.3±2.1	127.0±8.0	10.52±0.32	0.3074±0.0098
Pyroxene	900	0413B	0.371±0.019	34.7±2.0	328.8±5.3	10.45±0.17	0.323±0.025
1.00256 g	1750	0413C	0.0382±0.0060	24.5±1.6	97±18	11.34±0.27	1.286±0.037
Total			0.500±0.020	95.5±3.3	274.5±5.5	10.70±0.15	0.564±0.020
250406-15							
Pyroxene	900	P172A	0.268±0.014	52.5±2.9	451±28	10.24±0.21	0.315±0.022
0.43576 g	1750	P172B	0.0416±0.0079	15.7±1.3	203±50	11.67±0.33	2.03±0.19
Total			0.310±0.016	68.2±3.2	418±26	10.57±0.18	0.710±0.056
250406-16							
Pyroxene	900	P171A	0.1444±0.0076	26.1±1.6	907±40	10.25±0.17	0.315±0.018
0.44876 g	1750	P171B	0.0213±0.0072	9.4±1.1	430±140	13.21±0.51	3.13±0.30
Total			0.166±0.010	35.5±1.9	846±43	11.03±0.20	1.06±0.11
250406-17	600	0414A	0.1366±0.0071	21.2±1.3	170.2±4.8	10.34±0.23	0.313±0.018
Pyroxene	900	0414B	0.309±0.016	27.2±1.6	349.4±8.3	10.53±0.18	0.425±0.022
0.98118 g	1750	0414C	0.0490±0.0061	22.8±1.4	70.7±9.0	11.35±0.22	1.292±0.059
Total			0.495±0.019	71.2±2.5	272.3±6.6	10.74±0.12	0.669±0.026
240406-06 Olivine, 1.00167 g	Crush	K095	0.322±0.016	24.7±1.5	8.1±1.0	10.15±0.14	0.305±0.016

Sample	Temperature (°C)	File Name	^{4}He (10^{-8} cm^3/g)	^{20}Ne (10^{-12} cm^3/g)	$^{3}He/^{4}He$ (10^{-6})	$^{22}Ne/^{20}Ne$ (10^{-2})	$^{21}Ne/^{20}Ne$ (10^{-2})
240406-08 Olivine, 1.00230 g	Crush	K096	0.351±0.018	24.3±1.3	8.4±1.4	10.13±0.12	0.322±0.010
260406-20 Olivine, 1.02182 g	Crush	K094	0.414±0.021	27.1±1.6	8.7±1.0	10.27±0.12	0.304±0.017
250406-13 Pyroxene, 0.49752 g	Crush	K125	0.0046±0.0010	29.3±1.5	40^{+50}_{-40}	10.07±0.19	0.287±0.030
250406-17 Pyroxene, 1.00196 g	Crush	K118	0.01091±0.00066	30.9±2.0	21±10	10.24±0.15	0.300±0.017

[a] Technical difficulties occurred during He analyses.

Table 4. Predicted radiogenic ^{4}He and nucleogenic ^{3}He in Bar Ten olivine and pyroxene based on equations of Andrews (1985) and U, Th, and Li concentrations [ppm] determined by ICP-MS analyses, and assuming a 95 ka eruption age.

	U (ppm)	Th (ppm)	Li (ppm)	Predicted nucleogenic ^{3}He (at/g) (produced from Li)	Predicted radiogenic ^{4}He (10^9 at/g) (produced from U, Th)	Measured Total ^{4}He (10^9 at/g)	Radiogenic ^{4}He in Total measured ^{4}He (%)	Mantle ^{4}He in Total measured ^{4}He (%)[a]	Predicted Nucleogenic ^{3}He in Total measured ^{3}He (%)[b]	Mantle ^{3}He in Total measured ^{3}He (%)[c]	Cosmogenic ^{3}He in Total measured ^{3}He (%)[d]	Cosmogenic ^{3}He (10^6 atoms/g) after radiogenic/ nucleogenic corrections
OLIVINE												
051110-01	0.04	0.10	3.6	73	20	100.7	19	81	<0.001	2.4	97.6	28.5
240406-06	0.05	0.10	2.9	64	23	146.6	15	85	<0.001	4.0	96.0	26.0
240406-08	0.03	0.05	2.8	35	13	139.9	9	91	<0.001	3.6	96.4	29.8
240406-09	0.03	0.05	3.3	41	13	146.4	9	91	--	--	--	--
250406-16	0.04	0.18	3.1	86	25	239.7	11	89	<0.001	4.7	95.3	38.0
260406-20	0.04	0.12	2.4	53	21	878.2	2	98	<0.001	20.0	80.0	29.8
PYROXENE												
250406-15p	0.06	0.33	2.6	95	42	83.0	51	49	<0.001	1.0	99.0	35.6
250406-16p	0.03	0.26	2.1	53	28	44.5	63	37	<0.001	0.4	99.6	39.6
250406-17p	0.11	0.62	5.0	346	79	132.9	59	41	<0.001	1.2	98.8	37.7

Note: '--' indicates no available data.

[a]Values are based on the assumption that total measured ^{4}He = (mantle ^{4}He) +(radiogenic ^{4}He), and are the percentages remaining after subtracting the predicted radiogenic ^{4}He from total measured ^{4}He for each sample.

[b]Concentrations of B and Gd were not measured in this study, thus, any ^{3}He listed here as contributed through the $^6Li(n,\alpha)^3H(\beta^-)^3He$ reaction is an upper limit. B and Gd are neutron absorbers and thereby decrease the probability for neutrons to interact with Li.

[c]Mantle ^{3}He = (%Mantle ^{4}He)*(Total ^{4}He)* $(^3He/^4He)_{magmatic}$, where $(^3He/^4He)_{magmatic}$ = 6.06 R_a. This assumes all gas released during the crush is from mantle inclusions.

[d]Cosmogenic ^{3}He = (Total ^{3}He)-(Mantle ^{3}He)-(Predicted nucleogenic ^{3}He).

Table 5. Comparison of estimated $^{21}Ne_c$ production rates in pyroxene (based on a $^{40}Ar/^{39}Ar$ age of 80 ± 25 ka) to production rates derived from methods of Kober et al. (2005) and Masarik (2002) for Bar Ten pyroxene.

Pyroxene Sample	$P^{21}Ne_c$ [a] (at/g/yr) for $^{40}Ar/^{39}Ar$ = 80 ± 25 ka	Composition-based production rate (at /g/yr) Kober et al. (2005) method	Composition-based production rate (at /g/yr) Masarik (2002) method	Lal (1991) Scaling factor (from CosmoCalc)
250406-13	23	33	28	3.71
250406-15	26	32	28	3.62
250406-16	25	33	28	3.62
250406-17	26	33	28	3.36
Average	**25**	**33**	**28**	

[a] ± 31% uncertainty which mainly reflects the $^{40}Ar/^{39}Ar$ uncertainty, but also includes the uncertainty of the $^{21}Ne_c$ determination.

Table 6. $^{3}He_c$ and $^{21}Ne_c$ production rates for Bar Ten olivine and pyroxene, as derived by various methods described in the text.

		Kober $P^{3}He_c$ (at/g/yr)	Kober $P^{21}Ne_c$ (at/g/yr)	Masarik $P^{3}He_c$ (at/g/yr)	Masarik $P^{21}Ne_c$ (at/g/yr)	Cerling and Craig (1994) $P^{3}He_c$ (at/g/yr)	Poreda and Cerling (1992) $P^{21}Ne_c$ (at/g/yr)	$P^{21}Ne_c$ / $P^{3}He_c$	Composition-corrected $P^{3}He_c$ (at/g/yr) [a]	Composition - corrected $P^{21}Ne_c$ (at/g/yr) [b]	$P^{21}Ne_c$ / $P^{3}He_c$	Composition-corrected $P^{3}He_c$ (at/g/yr) [a]	Ratio-predicted $P^{21}Ne_c$ (at/g/yr) [c]	$P^{21}Ne_c$ / $P^{3}He_c$
Olivine	Fo content													
051110-01	82	164	58	108	54	118	45	0.381	119	46	0.387	119	48	0.400
240406-06	81	164	57	107	53	118	45	0.381	118	45	0.381	118	47	0.400
240406-08	81	164	57	107	53	118	45	0.381	118	45	0.381	118	47	0.400
240406-11	84	166	59	109	55	118	45	0.381	120	47	0.392	120	48	0.400
250406-16	82	164	58	108	54	118	45	0.381	119	46	0.387	119	48	0.400
260406-20	80	163	56	107	52	118	45	0.381	117	44	0.376	117	47	0.400
97-AZ-330-BT	84	166	59	109	55	118	45	0.381	120	47	0.392	120	48	0.400
Pyroxene	En content						This study $P^{21}Ne_c$ (at/g/yr) [d]							
250406-13	44	136	32	104	28	118	25	0.212	114	24	0.211	114	23	0.202
250406-15	43	135	32	104	28	118	25	0.212	114	24	0.211	114	23	0.202
250406-16	44	136	32	104	28	118	25	0.212	114	24	0.211	114	23	0.202
250406-17	44	136	32	104	28	118	25	0.212	114	24	0.211	114	23	0.202

Note: Fo= forsterite; En = Enstatite.

[a] $^{3}He_c$ production rates are corrected for elemental concentrations using Masarik (2002) and are normalized to 118 at/g/yr.

[b] $^{21}Ne_c$ production rates are corrected for elemental concentrations using Masarik (2002) and are normalized to 45 at/g/yr.

[c] $P^{21}Ne_c$ is 47-48 at/g/yr for olivine and 23 at/g/yr for clinopyroxene in Bar Ten flows, if composition-corrected $P^{3}He_c$ and $^{21}Ne_c$ /$^{3}He_c$ = 0.400 and 0.202 are accurate and valid for olivines and clinopyroxenes, respectively (see text for details). The $^{21}Ne_c$ /$^{3}He_c$ is based on values calculated from $^{21}Ne_c$ values in Table 1 and $^{3}He_c$ values from Table 4 (last column).

[d] estimated $P^{21}Ne_c$ in Bar Ten clinopyroxenes as obtained from the independent $^{40}Ar/^{39}Ar$ age of the upper flow.

Table 7. Calculation of factors used to normalize $^{3}He_c$ and $^{21}Ne_c$ production rates (P_{3Hec} and P_{21Nec}) in Masarik's (2002) scheme to experimentally calibrated production rates in olivine (Fo_{81}). P_{3Hec} and P_{21Nec} in Bar Ten olivines and pyroxenes are normalized to production rates of 118 ± 4 and 45 ± 4 at/g/yr in olivine Fo_{81}, which is the composition of the Tabernacle Hill olivine (Poreda and Cerling, 1992; Cerling and Craig, 1994).

Element	Atomic Mass (g/mol)	Masarik (2002) P_{3Hec} for each element (at/g/yr)	Masarik P_{3Hec} for each element in Fo_{81} (at/mol/yr)[a]	This Study Fo_{81}-normalized J_{3Hec} (at/g/yr)[b]	Masarik (2002) P_{21Nec} for each element in Fo_{81} (at/g/yr)	Masarik P_{21Nec} for each element in Fo_{81} (at/mol/yr) [a]	This Study Fo_{81}-normalized J_{21Nec} for Fo_{81} (at/g/yr) [b]
Na	22.990	--	--	--	102	--	86.8
O	15.999	128.7	8237	141.4	--	--	--
Mg	24.305	110.8	4362	121.8	175	6890	148.9
Al	26.982	102	--	112.1	62	--	52.8
Si	28.086	106	2977	116.5	42	1180	35.7
Ca	40.078	58	--	63.7	2	--	1.7
Fe	55.845	38.5	817	42.3	0.187	3.97	0.159
Ti	47.867	38.5	--	42.3	0.187	--	0.159
		Sum of Elemental Production Rates (at/mol/yr)	16393			8074	
		Sum Divided by Molecular weight of Fo_{81} (152.68 g/mol)	107.4			52.88	
		Normalization factor	1.099			0.851	

[a] $Fo_{81} = (Mg_{1.62}, Fe_{0.38})SiO_4$

[b] $J_i = P_i$ x normalization factor.

Table 8. $^{3}He_c$ and $^{21}Ne_c$ surface exposure ages of Bar Ten olivine and pyroxene, as derived by correcting experimentally determined $^{3}He_c$ production rates (Poreda and Cerling, 1992; Cerling and Craig, 1994) for elemental composition by normalizing with elemental production rates of Masarik (2002) and using experimental $^{21}Ne_c$ /$^{3}He_c$ values to correct $P^{21}Ne_c$ in olivine and pyroxene. **All ages are based on data reported in Table 1, except where noted (footnote d)**.

		Composition-corrected $P^{3}He_c$ (at/g/yr) [a]	Composition -corrected $P^{21}Ne_c$ (at/g/yr)	Composition -corrected $^{3}He_c$ age (ka)	Composition -corrected $^{21}Ne_c$ age (ka)
Olivine	Fo content				
051110-01	82	119	50 [b]	102±5	91±7
240406-06	81	118	49 [b]	93±5	97±7
240406-08	81	118	49 [b]	107±4	90±7
240406-11	84	120	51 [b]	96±5	94±5
250406-16	82	119	50 [b]	87±6	86±6
260406-20	80	117	48 [b]	96±5	98±6
97-AZ-330-BT	84	120	51 [b]	81±5	75±4
Pyroxene	En content				
250406-13	44	114	23 [c]	89±4	85±6
250406-15	43	114	23 [c]	86±7[d]	95±10
250406-16	44	114	23 [c]	96±7[d]	92±7
250406-17	44	114	23 [c]	98±7[d]	98±7

Note: All surface exposure ages in this table were determined using Lal's (1991) scaling factors as calculated by CosmoCalc (http://cosmocalc.googlepages.com; Vermeesch, 2007). Fo = forsterite; En = enstatite.

[a] $^{3}He_c$ production rates are corrected for elemental concentrations using Masarik (2002) and are normalized to 118 at/g/yr.

[b] $^{21}Ne_c$ production rates are corrected for elemental concentrations using Masarik (2002) and are normalized to 49 at/g/yr, based on age-agreement discussion in section 5.2.

[c] $^{21}Ne_c$ production rates are based on $P^{3}He_c$ that are corrected for elemental concentrations, using Masarik (2002) and are normalized to 118 at/g/yr, and the average $^{21}Ne_c/^{3}He_c$ value (=0.202) for Bar Ten pyroxenes (section 5.2; Table 6).

[d] Ages for these pyroxenes are based on $^{3}He_c$ concentrations in Table 4 (last column), which include corrections for radiogenic/nucleogenic helium contributions. Uncertainties do not include uncertainties in these corrections, but only uncertainties related to noble-gas analysis. If $^{3}He_c$ concentrations are used from Table 1, the following exposure ages are obtained: sample -15: 85±7 ka; sample -16: 95±7 ka; and sample -17: 97±7 ka.

Supplementary Data 1.

Sample 051110-02

Incremental Heating			36Ar(a)	37Ar(ca)	38Ar(cl)	39Ar(k)	40Ar(r)	Age ± 1σ (Ka)	40Ar(r) (%)	39Ar(k) (%)	K/Ca ± 1σ
06MQ210	700 °C		0.029115	0.016846	0.000140	0.013116	0.000000	0.0 ± 0.0	0.00	0.89	0.335 ± 0.035
06MQ211	750 °C		0.090031	0.139521	0.000000	0.075149	0.000000	0.0 ± 0.0	0.00	5.09	0.232 ± 0.013
06MQ212	800 °C	✓	0.077023	0.201035	0.000000	0.148523	0.024761	92.9 ± 174.0	0.11	10.07	0.318 ± 0.019
06MQ213	850 °C	✓	0.075073	0.479036	0.000000	0.348806	0.080013	127.9 ± 70.2	0.36	23.65	0.313 ± 0.017
06MQ214	900 °C	✓	0.048685	0.379335	0.000000	0.370645	0.089508	134.6 ± 60.9	0.62	25.13	0.420 ± 0.023
06MQ215	950 °C	✓	0.033795	0.269923	0.000000	0.252404	0.044384	98.0 ± 67.8	0.44	17.11	0.402 ± 0.023
06MQ216	1000 °C	✓	0.025882	0.190913	0.000000	0.138852	0.026030	104.5 ± 110.1	0.34	9.41	0.313 ± 0.018
06MQ217	1075 °C	✓	0.028897	0.218349	0.000000	0.127548	0.042091	184.0 ± 116.2	0.49	8.65	0.251 ± 0.015
06MQ218	1200 °C		0.001840	0.000462	0.000002	0.000000	0.000939	0.0 ± 0.0	0.17	0.00	0.000 ± 0.000
		Σ	0.410340	1.895421	0.000142	1.475044	0.307726				

Information on Analysis
CR22 - 051110/02
groundmass
furnace
BSHS
Project = GFZ06
Irradiation = VU57
J = 0.0003090 ± 0.0000009
DRA 1 = 25.260 ± 0.076 Ma

Results	40(r)/39(k) ± 1σ	Age ± 1σ (Ka)	MSWD	39Ar(k) (%,n)	K/Ca ± 1σ
Weighted Plateau	0.2220 ± 0.0605 ± 27.25%	123.8 ± 33.7 ± 27.25%	0.10	94.02 6	0.320 ± 0.025
		External Error ± 33.7	1.03	Statistical T Ratio	
		Analytical Error ± 33.7	1.0000	Error Magnification	
Total Fusion Age	0.2086 ± 0.0612 ± 29.34%	116.3 ± 34.1 ± 29.34%		9	0.017 ± 0.000
		External Error ± 34.1			
		Analytical Error ± 34.1			

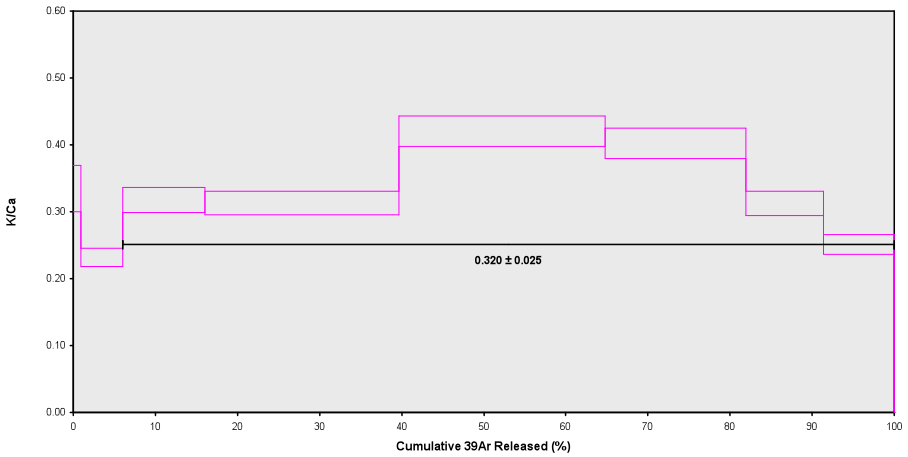

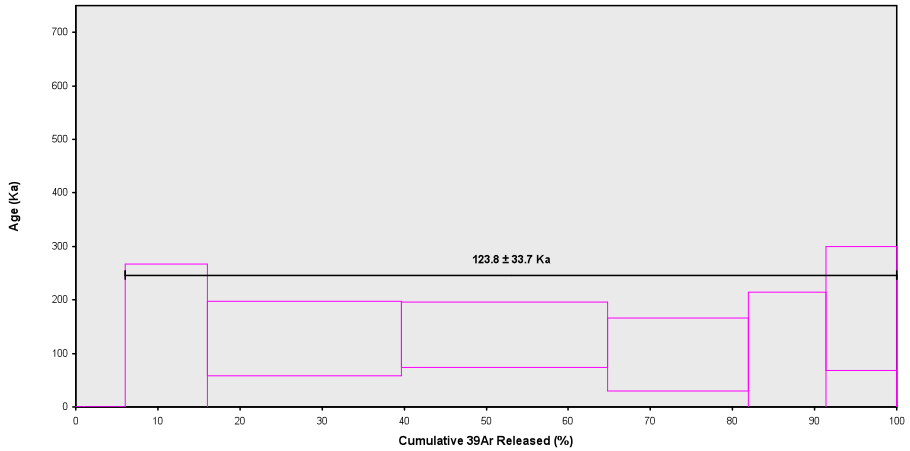

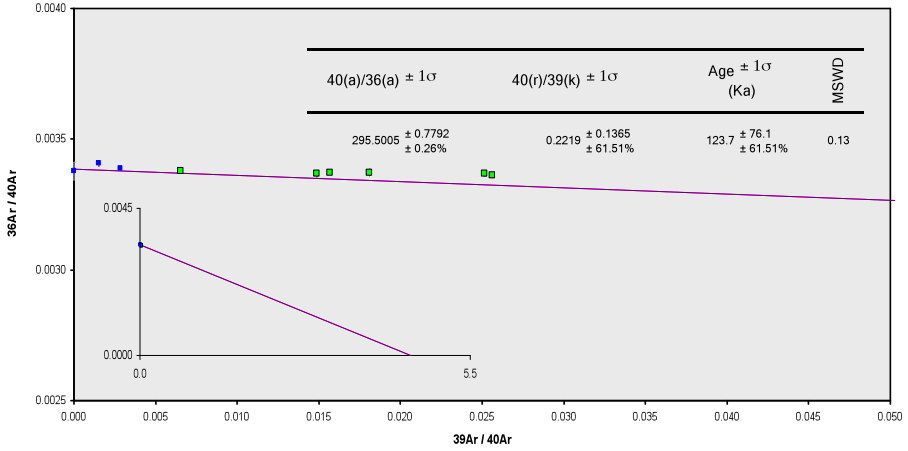

Supplementary Data 2.

Sample 051210-05

Incremental Heating			36Ar(a)	37Ar(ca)	38Ar(cl)	39Ar(k)	40Ar(r)	Age ± 1σ (Ka)	40Ar(r) (%)	39Ar(k) (%)	K/Ca ± 1σ
06MQ219	700 °C		0.018643	0.012534	0.000020	0.005201	0.000000	0.0 ± 0.0	0.00	0.27	0.178 ± 0.034
06MQ220	750 °C		0.066388	0.104416	0.000000	0.045219	0.000000	0.0 ± 0.0	0.00	2.38	0.186 ± 0.012
06MQ221	800 °C		0.058448	0.205029	0.000000	0.137229	0.000000	0.0 ± 0.0	0.00	7.22	0.288 ± 0.016
06MQ222	825 °C		0.045798	0.250178	0.000000	0.229177	0.000000	0.0 ± 0.0	0.00	12.06	0.394 ± 0.022
06MQ223	850 °C	✓	0.029671	0.225796	0.000000	0.243663	0.017303	39.6 ± 56.9	0.20	12.82	0.464 ± 0.026
06MQ224	875 °C	✓	0.025184	0.219640	0.000000	0.285499	0.066221	129.3 ± 48.0	0.88	15.03	0.559 ± 0.034
06MQ225	900 °C	✓	0.019397	0.179715	0.000000	0.249833	0.016413	36.6 ± 51.4	0.29	13.15	0.598 ± 0.035
06MQ226	950 °C	✓	0.022046	0.268804	0.000000	0.282253	0.037110	73.3 ± 43.3	0.57	14.85	0.452 ± 0.026
06MQ227	1000 °C	✓	0.020652	0.264821	0.000000	0.162389	0.041623	142.9 ± 76.7	0.68	8.55	0.264 ± 0.015
06MQ228	1100 °C		0.035245	0.473241	0.000000	0.158355	0.000000	0.0 ± 0.0	0.00	8.33	0.144 ± 0.008
06MQ229	1200 °C		0.032537	0.642136	0.000000	0.101241	0.048332	266.1 ± 167.7	0.50	5.33	0.068 ± 0.004
		Σ	0.374011	2.846312	0.000020	1.900060	0.227002				

Information on Analysis
CR23 - 051210/05
groundmass
furnace
BSHS
Project = GFZ06
Irradiation = VU57
J = 0.0003090 ± 0.0000009
DRA 1 = 25.260 ± 0.076 Ma

Results	40(r)/39(k) ± 1σ	Age ± 1σ (Ka)	MSWD	39Ar(k) (%,n)	K/Ca ± 1σ
Weighted Plateau	0.1431 ± 0.0420 ± 29.36%	79.8 ± 23.4 ± 29.37%	0.74	64.40 5	0.386 ± 0.063
		External Error ± 23.4	1.06	Statistical T Ratio	
		Analytical Error ± 23.4	1.0000	Error Magnification	
Total Fusion Age	0.1195 ± 0.0319 ± 26.67%	66.6 ± 17.8 ± 26.67%		11	0.015 ± 0.000
		External Error ± 17.8			
		Analytical Error ± 17.8